

BATIS: Bayesian Approaches for Targeted Improvement of Species Distribution Models

Catherine Villeneuve^{1,2}, Benjamin Akera^{1,2}, Mélisande Teng^{1,3}, David Rolnick^{1,2}

¹McGill University, ²Mila–Quebec AI Institute, ³Université de Montréal
catherine.villeneuve@mila.quebec

Abstract

Species distribution models (SDMs), which aim to predict species occurrence based on environmental variables, are widely used to monitor and respond to biodiversity change. Recent deep learning advances for SDMs have been shown to perform well on complex and heterogeneous datasets, but their effectiveness remains limited by spatial biases in the data. In this paper, we revisit deep SDMs from a Bayesian perspective and introduce BATIS, a novel and practical framework wherein prior predictions are updated iteratively using limited observational data. Models must appropriately capture both aleatoric and epistemic uncertainty to effectively combine fine-grained local insights with broader ecological patterns. We benchmark an extensive set of uncertainty quantification approaches on a novel dataset including citizen science observations from the eBird platform. Our empirical study shows how Bayesian deep learning approaches can greatly improve the reliability of SDMs in data-scarce locations, which can contribute to ecological understanding and conservation efforts.

Code — <https://github.com/cath34/batis>

Datasets — <https://huggingface.co/datasets/cathv/BATIS>

Extended version — <https://arxiv.org/abs/2510.19749>

1 Introduction

Understanding the factors governing the spatial distribution of species is a long-standing topic of interest in ecology (de Candolle 1855; Thuiller et al. 2015). The rapid loss of biodiversity further highlights the need to better understand species distributions and conservation status, which requires robust modeling methods (Sharma et al. 2025). *Species distribution models* (SDMs) are at the forefront of this research, enabling ecologists to predict and understand species occurrence by linking observational data (presence or absence) to environmental covariates (Elith and Leathwick 2009). These models have proved to be essential tools to support conservation planning and management (Jetz et al. 2019), with notable examples including predicting species range shift (Chauvier-Mendes et al. 2024), mapping invasive species risk (Davis et al. 2024), supporting translocation programs (Draper, Marques, and Iriondo 2019), reducing bycatch rates

in fisheries (Hazen et al. 2018), and informing IUCN Red List assessments (Syfert et al. 2014).

SDMs are traditionally based on statistical approaches, offering strong interpretability and theoretical grounding. However these methods often rely on restrictive assumptions such as linearity, leading them to struggle with high-dimensional datasets. Recently, deep learning approaches to SDMs proposed to overcome these challenges and were shown to consistently outperform statistical ecology methods for large and heterogeneous datasets (Deneu et al. 2021).

Although a wide variety of SDM approaches have now been introduced, their effectiveness at large spatio-temporal scales remains hindered by the abundance and geographical coverage of the data used to train them (Van Proosdij et al. 2016). In most cases, observations are disproportionately concentrated in areas easily accessible by roads (Kadmon, Farber, and Danin 2004) and with high human population densities (Speed et al. 2018). In contrast, remote locations are most often associated with very limited to no observations, as illustrated in Fig. 1.

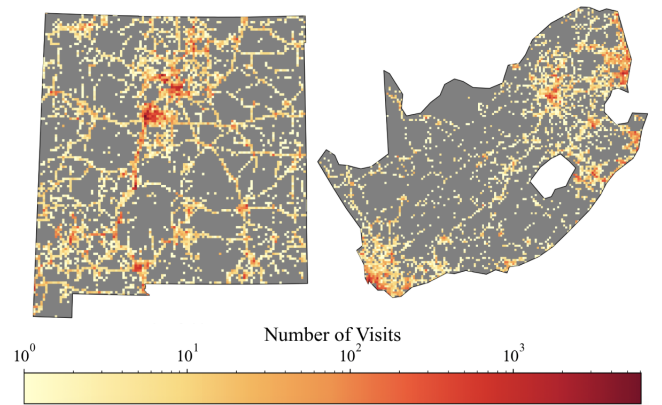


Figure 1: Distribution of citizen science sampling trips across New Mexico, US (left) and South Africa (right), retrieved from the eBird database for the whole year of 2024. The value assigned to each 5km² (US) and 10km² (South Africa) grid cell corresponds to the total number of visits that were registered within that cell.

Data distribution biases especially affect machine

learning-based approaches, which typically rely on trustworthy labeled data. Limited observations in a given location can lead to poor estimates of species occurrence (Fink et al. 2020) – essentially, noisy labels – and naïvely incorporating such data points in model training can degrade performance. However, sparse observations still offer potentially valuable information, and finding ways to properly leverage it could help improve SDMs and guide conservation efforts in remote or underresourced areas. We argue that uncertainty-aware methods can offer a principled way of leveraging limited location-specific observations, enabling controlled prediction updates that can balance global-scale models with local-scale observations.

In this work, we tackle the spatial heterogeneity challenge of biodiversity data by revisiting species distribution modeling from a Bayesian perspective, introducing **BATIS**, a framework enabling the application of **B**ayesian **A**pproaches for **T**argeted **I**mprovement of **S**pecies distribution models (named after the batis, a bird found in sub-Saharan Africa). In this framework, prior predictions from ML are iteratively refined offline with limited field observations in data-scarce locations, testing the ability of ML models to capture both the epistemic (model-inherent) and aleatoric (data-inherent) uncertainty of SDM data. Quantifying epistemic uncertainty provides a measure of the model’s confidence in its prior predictions and highlights how informative additional field observations could be, while measuring aleatoric uncertainty ensures that the noise associated with the additional data is appropriately taken into account. We present an empirical study of a variety of uncertainty-aware ML approaches approaches on this task, using a novel large-scale dataset.

- We introduce the framework of iteratively refining the prior predictions of an uncertainty-aware SDM with the help of limited additional on-the-ground information.
- We benchmark a variety of state-of-the-art uncertainty estimation ML methods on the above framework, and present a novel dataset derived from eBird (Sullivan et al. 2009), building on the SatBird (Teng et al. 2023) dataset.
- We find that our framework can rapidly improve predicted species distribution models in data-scarce locations, even with minimal additional ground truth data (<10 samples), effectively combining broader ecological patterns with fine-grained, location-specific insights.
- We provide evidence that machine learning approaches relying on aleatoric uncertainty are the most effective at improving predictions in low-data regimes.

BATIS can be seen as an innovative way of coupling the predictive power of modern deep learning to the statistical rigor of traditional hierarchical inference, thereby creating a bridge between ML and established methods in ecology. Our code and datasets are available open-source.

2 Related Works

Machine Learning for SDMs. Species distributions have been widely estimated from environmental data with statistical ecology methods. Popular SDMs in ecology include techniques based on maximum entropy (MaxEnt) (Phillips,

Dudík, and Schapire 2004), random forests (Valavi et al. 2021), and generalized linear models (Guisan, Edwards, and Hastie 2002). More recently, a wide variety of deep learning approaches have been introduced, including simple multi-layer perceptrons (Zbinden et al. 2024), computer vision methods leveraging remote sensing imagery (Estopinan et al. 2022; Teng et al. 2023) or location embeddings (Cole et al. 2023), and even language-based reasoning methods (Hamilton et al. 2024). Active learning (Lange et al. 2023) and few-shot learning (Lange et al. 2025) frameworks have also been introduced. Deep learning models have been shown to consistently outperform traditional approaches in ecology (Deneu et al. 2021), notably when applied to large-scale citizen science datasets (Davis et al. 2023).

Some deep learning-based SDMs have focused on estimating binary species range maps (Dorm et al. 2024). This corresponds to a multi-label classification problem in which the list of species that *can* be encountered at a given location is predicted, regardless of the frequency at which they are observed. Another important challenge is *encounter rate estimation*, i.e. a multi-output regression problem aimed at predicting the average rate at which observers encounter species at a given location (Johnston et al. 2021). The use of ML for predicting encounter rates has been explored in Teng et al. (2023) and Abdelwahed, Teng, and Rolnick (2024), a line of work which we follow here. Encounter rates are closely linked to the notion of *occupancy*, i.e. the probability of a species occupying a given site. Occupancy is a core concept in ecology (MacKenzie 2018), and understanding occupancy patterns is essential for prioritizing conservation efforts. Because encounter rates can be seen as the product of occupancy and detection probability (Johnston et al. 2021), they can provide a more nuanced and realistic representation of species distributions than binary range maps.

Bayesian Inference for SDMs. In statistical ecology, SDMs have been estimated in a Bayesian context using computationally intensive algorithms, such as Markov Chain Monte Carlo (MCMC) approaches (Zulian, Miller, and Ferraz 2021) and integrated nested Laplace approximation (Omre, Fjeldstad, and Forberg 2024). Golding and Purse (2016) proposed a more flexible approach based on Gaussian processes, but this was applicable only to a limited number of species and covariates. Our work is the first to reframe deep learning-based SDMs under a Bayesian perspective.

Uncertainty Quantification for SDMs. Uncertainty quantification is recognized by ecologists as a major challenge for SDMs (Yates et al. 2018). To date, however, the vast majority of works do not investigate the effects of uncertainty on model outputs (Zurell et al. 2020). Only a limited number of statistical tools have been proposed to measure and incorporate uncertainty estimates into SDMs (Beale and Lennon 2012), and these tools are not easily scalable, as they often require computationally expensive MCMC iterations to estimate posterior probability distributions (Rocchini et al. 2019). Thus, they are only appropriate for SDMs relying on a very small number of covariates and species. Approximation techniques such as model ensembling (Guo et al. 2015) have been applied to quantify

uncertainty in SDMs (Convertino et al. 2012), but their use remain limited. Recently, an active learning framework was proposed to sequentially select geographic locations that would best reduce uncertainty of an SDM for previously unmapped species Lange et al. (2023). This work however does not take a Bayesian approach to improving predictions, instead estimating uncertainty via disagreement across an ensemble of models to guide the active learning step.

Uncertainty Quantification in Deep Learning. An extensive variety of approaches have been proposed to approximate uncertainty in the Bayesian deep learning literature, since computing a posterior distribution over the parameters of a neural network according to the rule of Bayesian inference is analytically intractable (Band et al. 2021). However, these approaches have mostly been tested on generic vision benchmarks (Mucsányi, Kirchhof, and Oh 2024) such as CIFAR-10 (Krizhevsky 2009) and ImageNet-1k (Deng et al. 2009), which do not reflect the complexity of real-world tasks. Our work is the first to integrate such approaches for solving a complex ecological task.

3 The BATIS Framework

Species Encounter Rate Estimation

We here formalize the problem of species distribution modeling in the context of checklist-based surveys (presence-absence data) from ecologists and/or citizen science platforms. Let L be a region of interest, and $\mathcal{S} = \{s_1, \dots, s_N\}$ be a set of N species that may potentially exist within L . We consider observations within L as occurring at one of a set of K discrete *hotspots* $\mathcal{H} = \{h_1, \dots, h_K\}$, each representing an area in which observers can record species (e.g. a park, geographic feature, or address). To each hotspot $h_k \in \{1, \dots, K\}$ is associated a set of checklists $\mathcal{C}_k = \{\mathbf{c}_j\}_{j=1}^{|\mathcal{C}_k|}$, where each checklist $\mathbf{c}_j \in \{0, 1\}^N$ indicates which of the N species are recorded as present (1) or absent (0) during an observer’s visit to the location. For any (non-empty) set \mathcal{C}_k we define $p_{i,k}$ of species i at hotspot k to be the rate at which i is reported across checklists:

$$p_{i,k} := \frac{1}{|\mathcal{C}_k|} \sum_{\mathbf{c}_j \in \mathcal{C}_k} \mathbf{c}_{i,j} \quad (1)$$

It is a standard assumption that as $|\mathcal{C}_k| \rightarrow \infty$ (assuming a diversity of observers, observation dates, etc.), the value $p_{i,k}$ converges to an ecological quantity, the *encounter rate* $p_{i,k}^\infty$, representing the chance that a random observer will encounter species i at h_k on any given occasion.

Following Teng et al. (2023); Abdelwahed, Teng, and Rolnick (2024), we consider a machine learning formulation of species distribution modeling in which the encounter rate $p_{i,k}^\infty$ is to be estimated for each species i , given a set of information associated with the hotspot h_k – e.g., average precipitation, temperature, etc., as well as satellite imagery of the location. In practice, of course, the ground truth value $p_{i,k}^\infty$ is not directly observable, but is well-approximated by $p_{i,k}$ for hotspots h_k where $|\mathcal{C}_k|$ is sufficiently large; therefore the task is to estimate $p_{i,k}$.

Bayesian Estimates of Encounter Rates

For hotspot $h_k \in \mathcal{H}$, let $C_{i,k} = p_{i,k} \cdot |\mathcal{C}_k|$ be the number of times species i was observed at h_k . Then, we may assume that $C_{i,k}$ follows a binomial distribution parameterized by the true encounter rate – i.e. $C_{i,k} \sim \text{Binomial}(J, p_{i,k}^\infty)$. This simple assumption allows us to formulate a *Bayesian inference problem*, in which we place a *Beta prior* over $p_{i,k}^\infty$:

$$p_{i,k}^\infty \sim \text{Beta}(\alpha_{i,k}, \beta_{i,k}) \quad (2)$$

Instead of estimating $p_{i,k}^\infty$ directly, we may consider instead the problem of estimating the parameters $\alpha_{i,k}$ and $\beta_{i,k}$, which can be defined by the closed-form equations

$$\alpha_{i,k} = \mu_{i,k} \left(\frac{\mu_{i,k}(1 - \mu_{i,k})}{\sigma_{i,k}^2} - 1 \right) \quad (3)$$

$$\beta_{i,k} = (1 - \mu_{i,k}) \left(\frac{\mu_{i,k}(1 - \mu_{i,k})}{\sigma_{i,k}^2} - 1 \right) \quad (4)$$

where at each point $\mu_{i,k} \in [0, 1]$ encodes our best estimate of the encounter rate of species i at h_k , and $\sigma_{i,k}^2 \leq \mu_{i,k}(1 - \mu_{i,k})$ encodes our uncertainty about that belief.

While previous approaches of predicting species distributions using environmental variables made it possible to estimate encounter rates at a location without incorporating observations at the location, our Bayesian framework makes it possible to combine broad patterns learned by the SDM with any individual checklists recorded at the location in question. Namely, we may consider the output of an SDM to be an initial estimate of $\alpha_{i,k}$ and $\beta_{i,k}$, and we may then incorporate additional information from a checklist of observations by performing a Bayesian update to these parameters to obtain the posterior. In the Beta distribution, this update takes a convenient form: $\alpha_{i,k} := \alpha_{i,k} + \sum_{\mathbf{c}'_j \in \mathcal{C}'_k} \mathbf{c}'_{i,j}$ and $\beta_{i,k} := \beta_{i,k} + 1 - \sum_{\mathbf{c}'_j \in \mathcal{C}'_k} \mathbf{c}'_{i,j}$.

Our Bayesian reformulation of the species distribution modeling problem thus allows us to iteratively update prior encounter rates predictions coming from an ML model with additional field observations as they are recorded.

Applications

Our approach can significantly improve encounter rate predictions in data-scarce regions (see section 5). Specifically, our framework is useful since, due to the geographic distribution of species observational data, most locations have a small but meaningful number of observations – that is, there are insufficient observations to reliably calculate the encounter rate empirically, yet enough observations that they contain valuable information. BATIS is particularly well-suited for location-specific ecological questions, such as assessing changes in habitat use and monitoring threatened species presence in protected areas. Moreover, because it allows for fast and lightweight updates of prior predictions, our framework is ideal for integrating daily or weekly updates from citizen science databases such as eBird or iNaturalist (iNaturalist), which are continuously growing, into the SDMs used to inform conservation and land use decisions.

4 The BATIS Benchmark

Dataset

We introduce a dataset for the BATIS framework. We rely on the eBird citizen science database (Sullivan et al. 2009), containing millions of bird observations across the globe standardized in the form of *checklists*, indicating which species were seen or not during a given survey trip. This large amount of data allows us to create a benchmark of test cases that mirrors the real-world scenarios in which BATIS can be applied. We can notably simulate data-deficient locations by providing partial information to SDM algorithms so as to test their generalization capabilities against full ground-truth data. Although eBird strictly focuses on birds, its structure and scale makes it an ideal setting for evaluating BATIS methods, which we hope may then be applied to less standardized datasets, such as those available through GBIF.

Following Teng et al. (2023), we first extracted complete checklists from all hotspots associated with the mainland portions of Kenya (KE), South Africa (ZA), and the contiguous United States. For the US, we followed the same approach as Teng et al. (2023), splitting the dataset into two seasons: summer (US-S, breeding period) and winter (US-W, non-breeding period). We did not consider seasonality for the KE and ZA datasets, as these regions have significantly fewer available checklists and seasonal migrations are also less pronounced in KE and ZA than in the US. Table 1 summarizes the composition of each subdataset. Further details on the dataset can be found in Appendix A.

	KE	ZA	US-W	US-S
Start Date	01/01/10	01/01/18	01/12/22	01/06/22
End Date	31/12/23	17/06/24	31/01/23	31/07/22
N. Species	1,054	755	670	670
N. Hotspots	8,551	6,643	45,882	98,443
N. Checklists	44,852	498,867	3,673,742	3,920,846

Table 1: Summary of the composition of the four subdatasets

Remote Sensing Variables. Our dataset also includes bioclimatic rasters from the WorldClim2.1 model (1km resolution) and Sentinel-2 satellite images (10m resolution) for each hotspot. These serve as predictive variables (inputs) to the models we test, and were selected based on the work of Teng et al. (2023). More information on these variables can be found in Appendix A.

Splits. We reserved 50% of the hotspots with ≥ 15 checklists for the test set (15 being a large enough value to reliably estimate the true encounter rate $p_{i,k}^\infty$). The remaining hotspots were split into training and validation sets in a 80:20 ratio, and we used DBSCAN to cluster hotspots and proportionally distribute them across splits, which prevents auto-correlation and over-fitting (Roberts et al. 2017). Table 5 (Appendix A) summarizes the content of each split.

Uncertainty-Agnostic Methods

We considered four SDM baselines in our benchmark. The first one, referred to as **Mean Encounter Rate**, simply predicts the average encounter rate on the training set for each species, ignoring the inputs. We also include a **Random Forest** baseline trained from bioclimatic variables only, as this is a frequently used approach in ecology. Because bioclimatic variables are still almost always exclusively used in ecology, we include a **Multi-Layer Perceptron Model (MLP)** solely trained from these inputs. Finally, we consider the **ResNet-18** approach introduced by Teng et al. (2023), as it was shown to be the best performing model among the Sat-Bird benchmark. The ResNet-18 relies on both bioclimatic variables and satellite imagery as inputs. More information on each of our SDM baselines can be found in Appendix F.

Uncertainty-Aware Methods

We considered the uncertainty estimation approaches listed below. Except for the Fixed and Historical Variance baselines, we restricted ourselves exclusively to distributional approaches, as they offer a more principled way of estimating both the mean and variance of each predicted encounter rate (Mucsányi, Kirchhof, and Oh 2024). More details on each approach can be found in Appendix F.

Fixed Variance. Let $\hat{\mu}$ be the encounter rate predicted by an SDM. Our Fixed Variance (FV) baseline directly considers $\hat{\mu}$ as the mean, and fixes a pre-determined variance $\hat{\sigma}^2$ to initialize the prior. The pre-determined variance must be contained within $\hat{\sigma}^2 \leq \hat{\mu}(1 - \hat{\mu})$ to maintain a valid Beta distribution. FV also includes a hyperparameter $\tau \in (0, 1]$ to finetune $\hat{\sigma}^2$ more easily:

$$\hat{\sigma}^2 = \tau \cdot \hat{\mu}(1 - \hat{\mu}). \quad (5)$$

We considered $\tau = 1$ in our experiments, as we were interested in investigating the behavior of FV when the non-informative Beta(0, 0) distribution is assigned as the prior.

Historical Variance. Our Historical Variance (HV) baseline computes $\hat{\sigma}^2$ from past checklists instead, which can be viewed as a way of trying to integrate the uncertainty associated with the data collection process into our framework. In edge cases where $\hat{\sigma}^2 > \hat{\mu}(1 - \hat{\mu})$, the variance is instead fixed at $\hat{\sigma}^2 = \hat{\mu}(1 - \hat{\mu})$. In our experiments, we limited the number of past checklists used to compute the prior variance to 5, as we are interested in how this method performs in a low-data regime.

Monte-Carlo Dropout (Gal and Ghahramani 2016). MC Dropout (MCD) can be shown to be a variational approximation of a deep Gaussian process (Gal and Ghahramani 2016). A proportion of neurons are randomly deactivated at training and test time, and M forward passes are used to compute mean and variance for each location. MCD is primarily effective at capturing epistemic uncertainty.

Deep Ensembles (Lakshminarayanan, Pritzel, and Blundell 2017). In Deep Ensembles (DE), an ensemble of M

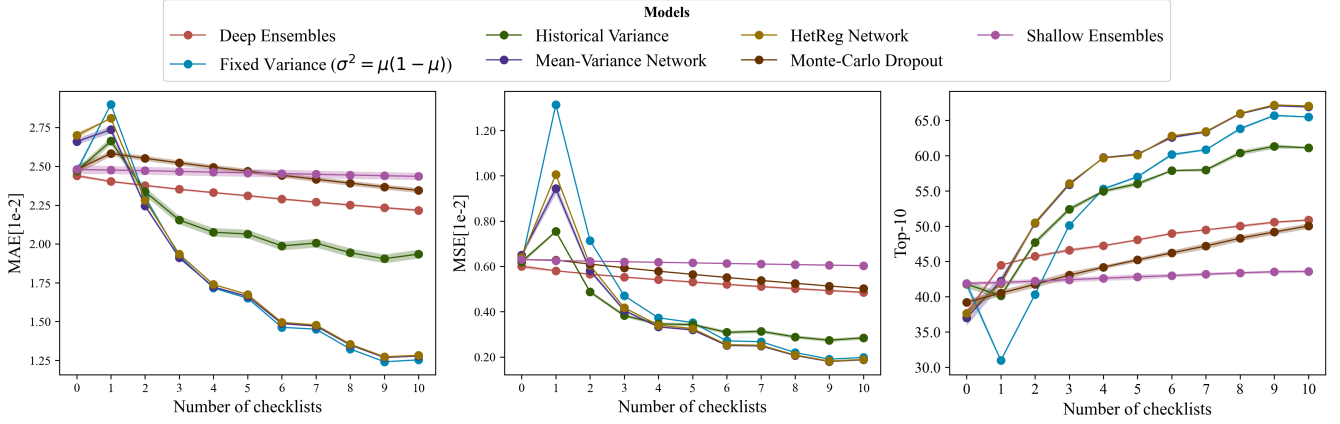


Figure 2: Iterative improvements for the different uncertainty estimation approaches with increasing number of checklist updates for the MAE, MSE and Top-10 metrics on the South Africa Region test set. We report the mean on three seeds and standard deviations for each model.

neural networks are independently trained on the same task, and their individual predictions on the same input can be used to estimate mean and variance. Despite its simplicity, DE is the current state-of-the-art for estimating epistemic uncertainty in deep learning (Mukhoti et al. 2021).

Shallow-Ensembles (Lee et al. 2015). Shallow Ensembles (SE) aim to offer a computationally cheaper alternative to DE by using a shared backbone and M output heads. The mean and variance of each predictions can be estimated by averaging the outputs of the M heads.

Mean-Variance Network (Nix and Weigend 1994; Sluiterman, Cator, and Heskes 2023). A Mean-Variance Network (MVN) maps each location to two outputs: a predicted mean encounter rate vector and a predicted variance vector. The predicted variance can be considered as a measure of aleatoric uncertainty, as it aims to reflect the inherent task difficulty. MVNs are trained using the Gaussian negative log-likelihood loss function, presuming that encounter rates are normally distributed, which results in an increase in predicted variance when the predicted mean encounter rate differs greatly from the ground truth value.

Heteroscedastic Regression Neural Network (Kendall and Gal 2017). A Heteroscedastic Regression Neural Network (HetReg) is very similar to an MVN, but adds MC Dropout sampling to simultaneously quantify aleatoric and epistemic uncertainty. M dropout passes are used to compute the mean encounter rate vector, and variance is estimated by adding epistemic uncertainty (variance computed from M predicted encounter rates) to aleatoric uncertainty (mean computed from M predicted variances).

Experiments

We performed the experiments described below. Training protocol details, including hyperparameters, and compute resources can be found in Appendix G.

Overall performance. We trained each model on each of the four subdatasets. We report baseline performance for each model in Table 2. Then, we investigate how the framework introduced in section 3 with the uncertainty quantification approaches described in section 4 can improve these baseline results. We report performance after updating the posterior distribution of each hotspot with five new checklists for each model.

Region-specific episodic behavior. We investigate the episodic behavior of our proposed Bayesian framework for the MLP and ResNet-18 models. We study how average performance evolves as we iteratively update the posterior distributions associated with each hotspot of our test set, for up to ten checklists.

Species-specific episodic behavior. We study how our proposed framework can be potentially leveraged to improve the reliability of range maps for individual species in low-data regimes. To do so, we consider how the absolute error between the predicted and ground truth encounter rates for a single species changes as we iteratively update the posterior distribution across an entire region.

Metrics. We evaluate our methods with the same metrics as Teng et al. (2023), namely MAE, MSE, Top-10, Top-30, and Top-k accuracy. Further details on these metrics are provided in Appendix G.

5 Results and Discussion

Overall results. Table 2 details the performance of uncertain-agnostic and uncertainty-aware models on the KE and ZA subdatasets. Results for the US can be found in Tables 10 and 11 in Appendix H. We observe that uncertainty-aware methods significantly outperforms all the uncertainty-agnostic approaches on our test set, even when prior predictions are updated with five checklists only. This suggests that our Bayesian approach to SDM estimation could greatly improve the reliability of predictions in data-scarce locations.

Our proposed framework essentially merges the strengths of traditional tools for Earth-scale mapping, which can make estimates for large regions with high throughput, and of ground-based surveys, which can record specific and accurate data with high effort.

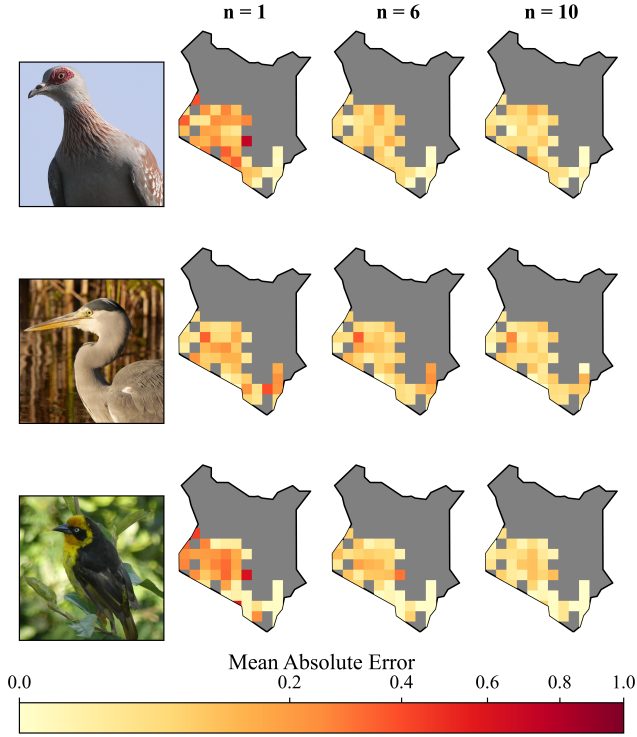


Figure 3: Evolution of the MAE in relation to the number of checklists (1, 6, 10) used to update the posterior distribution for three bird species of Kenya (*Columba guinea*, *Ardea cinerea*, *Ploceus baglafecht*). The value assigned to each 70km² grid cell corresponds to the mean MAE computed on the aggregation of all the hotspots located within that cell.

Iterative Improvements by Region. Figure 2 shows the evolution of the performance of the uncertainty-aware approaches with increasing number of checklist updates, on the ZA subdataset. Similar figures for the KE and US subdatasets are provided in Appendix H. We observe that our Bayesian framework requires as few as one or two checklists to significantly outperform static baselines. MVN and HetReg are the top-performing methods in our benchmark, with HetReg performing only marginally better than MVN. This is likely because HetReg and MVN share a common aleatoric uncertainty quantification module, but HetReg also includes an epistemic uncertainty estimation module. Estimating epistemic uncertainty alone, however, does not significantly improve on static baselines, as demonstrated by the limited improvements in performance with Deep Ensembles. Our findings are consistent across all four subdatasets. Interestingly, we also observe that the Fixed Variance baseline reaches MAE and MSE performance comparable to HetReg/MVN after 10 checklists, when the prior variance

is fixed to its maximum theoretical value.

Iterative Improvements by Species. As shown in Fig. 3, our approach rapidly improves encounter rate predictions for species in data-scarce locations. The error quickly drops as more checklists update the posterior distributions, and the improvements are consistent across all hotspots. Our approach shows potential for generating more reliable range maps in areas where a given species has been observed only a handful of times. This could be especially valuable for conservationists monitoring rare or endangered species in areas where gathering additional observations is challenging.

Aleatoric vs. epistemic uncertainty. We find that models relying on aleatoric uncertainty (such as HetReg and MVN) perform better than those which rely on epistemic uncertainty (such as DE and MCD). This likely results from two factors: First, with real-world observation-based data, similar conditions can occur with very different observations (in this case, reflecting variability in the whereabouts of individual animals and their visibility to an observer). Second, subtle environmental differences may not be fully captured by the input variables. Our conclusions are consistent with trends noted in the Bayesian ML literature (Kendall and Gal 2017), in which it is observed that epistemic uncertainty can be poorly estimated in deep learning models due to the implicit assumption that similar inputs lead to similar outcomes. By contrast, aleatoric uncertainty estimation approaches allow us to capture the inherent unpredictability of species observations and the potential existence of local environmental factors not captured by the prior SDM.

6 Limitations

Effectively combining large-scale ecological patterns with local information remains challenging. There remains tension between the broad environmental variables learned by deep SDMs (our Bayesian prior) and the hotspot-specific features captured by observational information (our updates to that prior). As shown in Figure 2, the initial predictions of an uncertainty-aware SDM can be overwritten in a first Bayesian update, when the estimated prior variance is large. This can lead to an initial drop in performance before enough updates are performed to boost performance, even though performance would ideally increase *monotonically* with number of updates. A simple approach to mitigate such behavior is to consider a weighted average of predictions from the prior and the updated SDM, progressively giving more importance to the updates with more observations. We provide additional experiments showing how such an approach can help smooth the results curve observed in Fig. 2 in Appendix E..

Uncertainty estimation approaches cannot fully correct for biases in citizen science data. Citizen science data is heavily influenced by *predictable* factors such as the day of the week, the time of day, the expertise of the observer, the weather, and the proximity to population centers (Sierra et al. 2025). Such biases are *structured*, which technically violates the randomness assumption of aleatoric uncertainty. Epistemic uncertainty estimation approaches can potentially

	MAE[1e-2]		MSE[1e-2]		Top-10		Top-30		Top-k	
Kenya										
MER	3.94		0.82		1.79		2.63		16.21	
MLP	3.51±0.01		0.81±0.00		0.92±0.07		2.18±0.13		16.92±0.04	
Random Forest	3.57±0.00		1.00±0.00		0.31±0.01		2.05±0.02		17.23±0.01	
ResNet-18	1.87±0.04		0.35±0.01		41.24±1.82		52.93±1.54		68.04±0.75	
ResNet-18+FV	1.87	1.50	0.35	0.26	41.24	51.71	52.93	64.46	68.82	75.26
	±0.04	±0.00	±0.01	±0.00	±1.82	±0.26	±1.54	±0.31	±0.75	±0.63
ResNet-18+HV	1.87	1.67	0.35	0.24	41.24	54.68	52.93	63.03	68.82	65.82
	±0.04	±0.03	±0.01	±0.01	±1.82	±0.43	±1.54	±0.63	±0.75	±0.70
ResNet-18+MVN	2.04	1.52	0.37	0.24	36.33	57.98	48.90	67.97	66.38	61.46
	±0.11	±0.03	±0.01	±0.00	±1.07	±0.10	±1.23	±0.17	±0.82	±2.45
ResNet-18+HetReg	2.04	1.52	0.37	0.25	36.24	57.98	49.11	67.82	66.67	61.19
	±0.02	±0.01	±0.01	±0.00	±1.06	±0.13	±0.53	±0.09	±0.12	±0.60
ResNet-18+DE	1.81	1.75	0.32	0.29	44.34	48.47	56.06	59.54	69.94	70.41
	±0.04	±0.06	±0.01	±0.01	±0.31	±1.06	±0.63	±1.48	±0.53	±0.56
ResNet-18+MCD	1.91	1.82	0.37	0.33	38.65	43.15	50.18	54.36	67.18	68.30
	±0.01	±0.01	±0.01	±0.01	±1.19	±1.01	±0.63	±0.81	±0.11	±0.19
ResNet-18+SE	1.73	1.71	0.33	0.32	43.53	44.19	55.79	56.49	70.47	70.70
	±0.01	±0.01	±0.00	±0.00	±0.26	±0.08	±0.41	±0.44	±0.16	±0.16
South Africa										
MER	3.62		0.84		25.53		36.87		49.31	
MLP	2.87±0.00		0.71±0.00		35.17±0.15		51.18±0.4		61.72±0.10	
Random Forest	2.54±0.01		0.69±0.00		38.21±0.16		54.23±0.20		64.26±0.09	
ResNet-18	2.47±0.02		0.62±0.01		41.79±0.59		57.20±0.32		67.11±0.23	
ResNet-18+FV	2.47	1.65	0.62	0.35	41.79	57.00	57.20	69.59	67.11	79.90
	±0.02	±0.00	±0.01	±0.00	±0.59	±0.17	±0.32	±0.12	±0.23	±0.13
ResNet-18+HV	2.47	2.06	0.62	0.34	41.79	56.00	57.20	67.55	67.11	70.79
	±0.04	±0.02	±0.00	±0.00	±0.59	±0.32	±0.32	±0.23	±0.23	±0.13
ResNet-18+MVN	2.66	1.66	0.65	0.32	37.01	60.19	53.20	70.68	64.61	71.88
	±0.02	±0.00	±0.01	±0.00	±1.12	±0.16	±1.06	±0.17	±0.27	±0.35
ResNet-18+HetReg	2.70	1.67	0.64	0.32	37.63	60.10	53.65	70.5	64.84	71.0
	±0.02	±0.00	±0.00	±0.00	±0.58	±0.03	±0.18	±0.04	±0.17	±0.30
ResNet-18+DE	2.44	2.31	0.60	0.53	43.30	48.06	58.47	62.11	67.84	69.72
	±0.01	±0.01	±0.00	±0.00	±0.13	±0.12	±0.06	±0.22	±0.13	±0.09
ResNet-18+MCD	2.61	2.47	0.64	0.56	39.21	45.21	55.00	59.22	65.64	67.86
	±0.01	±0.01	±0.00	±0.00	±0.44	±0.30	±0.40	±0.35	±0.16	±0.20
ResNet-18+SE	2.48	2.46	0.63	0.61	41.90	42.80	56.93	57.67	67.09	67.48
	±0.03	±0.02	±0.00	±0.00	±0.22	±0.39	±0.10	±0.13	±0.09	±0.06

Table 2: Performance of SDM-estimation approaches both **without Bayesian updates** (left side in split columns) and **after updates from five checklists** (right side). Note that the first four methods for each region are not uncertainty-aware and therefore cannot be updated with checklist information. Means are shown \pm standard deviation across runs. (Note that many standard deviations are quite low; those reported as 0.00 are accurate.)

correct for biases if they can be explicitly modeled, but are unable to do so if they are not encoded in the data. While our work shows that is possible to compensate partially for data gaps associated with the irregular distribution of citizen science data, some biases may affect the accuracy of the underlying numbers used as ground truth, which cannot be compensated for by such methods and remain an active object of inquiry in statistical ecology (Rocchini et al. 2023).

7 Conclusion

In this work, we presented BATIS, a novel framework for species distribution modeling in which uncertainty-aware

machine learning approaches are iteratively refined with additional on-the-ground information. Our results show how our framework can rapidly improve SDM predictions in data-scarce locations by combining broader ecological patterns with fine-grained, location-specific insights. Our study also suggests that ML approaches focusing on aleatoric uncertainty provide a better measure of observational variability than those focusing on epistemic uncertainty.

Pathway to impact. SDMs are widely used to inform decisions in conservation, land use, and other areas of impact (Jetz et al. 2019). We hope that BATIS can improve the ac-

curacy of such SDMs in applications where new observations are continually arriving, such as the monitoring of protected areas and endangered species, as well as guiding policies in underresourced or remote regions with lower data availability. Our framework is designed to be readily integrated into existing workflows for creation and utilization of SDMs. In addition, traditional barriers to integration of deep learning into ecology have included computational cost and lack of perceived interpretability. Our proposed approach is computationally lightweight and allow for improved performance without costly retraining, while the focus on uncertainty quantification makes model predictions more transparent, as well as bringing the output closer to the statistical tools already familiar to those working with SDMs.

Future work. Future work includes extending BATIS to guide sampling effort in citizen science initiatives, in collaboration with ecologists, and investigating the behavior of different uncertainty estimation approaches with presence-only data (which are often more abundant and readily available than presence-absence checklist data ; Zbinden et al. (2024)). Finally, an impactful extension of our work would be to control for additional sources of biases in the data, e.g. building on Sierra et al. (2025) by considering subdatasets labeled according to different types of bias.

Acknowledgments

We would like to thank members of the Rolnick lab and Lauren Harrell for feedback on earlier versions of this work and for helpful discussions. This work was partly supported by the Global Center on AI and Biodiversity Change (US NSF OISE-2330423 and Canada NSERC 585136) and the Canada CIFAR AI Chairs program. Catherine Villeneuve is also supported by an NSERC CGS-D fellowship (Award No. 589535). We also acknowledge computational support from the Digital Research Alliance of Canada and from Mila - AI Quebec AI Institute, including material support from NVIDIA Corporation.

References

Abdelwahed, H. R.; Teng, M.; and Rolnick, D. 2024. Predicting Species Occurrence Patterns from Partial Observations. In *Tackling Climate Change with Machine Learning at ICML*.

American Birding Association ; Checklists of the continental United States. n.d. <https://www.aba.org/aba-checklist/>. Accessed : 2024-12-01.

Avibase - The World Bird Database. n.d. <https://avibase.bsc-eoc.org/avibase.jsp?lang=EN>. Accessed : 2024-12-01.

Band, N.; Rudner, T. G. J.; Feng, Q.; Filos, A.; Nado, Z.; Dusenberry, M.; Jerfel, G.; Tran, D.; and Gal, Y. 2021. Benchmarking Bayesian Deep Learning on Diabetic Retinopathy Detection Tasks. In *Proc. of the Neural Information Processing Systems Track on Datasets and Benchmarks*.

Beale, C. M.; and Lennon, J. J. 2012. Incorporating uncertainty in predictive species distribution modelling. *Philosophical Transactions of the Royal Society B: Biological Sciences*, 367: 247–258.

BirdLife - Bird Checklists of South Africa. n.d. <https://www.birdlife.org.za/media-and-resources/bird-checklists/>. Accessed : 2025-03-01.

Chauvier-Mendes, Y.; Pollock, L. J.; Verburg, P. H.; Karger, D. N.; Pellissier, L.; Lavergne, S.; Zimmermann, N. E.; and Thuiller, W. 2024. Transnational conservation to anticipate future plant shifts in Europe. *Nature Ecology & Evolution*, 8(3): 454–466.

Cole, E.; Deneu, B.; Lorieul, T.; Servajean, M.; Botella, C.; Morris, D.; Jojic, N.; Bonnet, P.; and Joly, A. 2020. The GeoLifeCLEF 2020 Dataset. arXiv:2004.04192.

Cole, E.; Van Horn, G.; Lange, C.; Shepard, A.; Leary, P.; Perona, P.; Loarie, S.; and Mac Aodha, O. 2023. Spatial Implicit Neural Representations for Global-Scale Species Mapping. In *ICML*.

Convertino, M.; Welle, P.; Muñoz-Carpena, R.; Kiker, G. A.; Chu-Agor, M.; Fischer, R. A.; and Linkov, I. 2012. Episodic uncertainty in predicting shorebird biogeography affected by sea-level rise. *Ecological Modelling*, 240: 1–15.

Davis, A. J. S.; Groom, Q.; Adriaens, T.; Vanderhoeven, S.; De Troch, R.; Oldoni, D.; Desmet, P.; Reyserhove, L.; Lens, L.; and Strubbe, D. 2024. Reproducible WiSDM: a workflow for reproducible invasive alien species risk maps under climate change scenarios using standardized open data. *Frontiers in Ecology and Evolution*, 12: 1148895.

Davis, C. L.; Bai, Y.; Chen, D.; Robinson, O.; Ruiz-Gutierrez, V.; Gomes, C. P.; and Fink, D. 2023. Deep learning with citizen science data enables estimation of species diversity and composition at continental extents. *Ecology*, 104(12): e4175.

de Candolle, A. 1855. *Géographie botanique raisonnée; ou, Exposition des faits principaux et des lois concernant la distribution géographique des plantes de l'époque actuelle*. Masson.

Deneu, B.; Servajean, M.; Bonnet, P.; Botella, C.; Munoz, F.; and Joly, A. 2021. Convolutional neural networks improve species distribution modelling by capturing the spatial structure of the environment. *PLOS Computational Biology*, 17(4).

Deng, J.; Dong, W.; Socher, R.; Li, L.-J.; Li, K.; and Fei-Fei, L. 2009. ImageNet: A large-scale hierarchical image database. In *2009 IEEE Conference on Computer Vision and Pattern Recognition*, 248–255.

Dorm, F.; Lange, C.; Loarie, S.; and Aodha, O. M. 2024. Generating Binary Species Range Maps. arXiv:2408.15956.

Draper, D.; Marques, I.; and Iriondo, J. M. 2019. Species distribution models with field validation, a key approach for successful selection of receptor sites in conservation translocations. *Global Ecology and Conservation*, 19: e00653.

Elith, J.; and Leathwick, J. R. 2009. Species Distribution Models: Ecological Explanation and Prediction Across Space and Time. *Annual Review of Ecology, Evolution, and Systematics*, 40(1): 677–697.

- Estopinan, J.; Servajean, M.; Bonnet, P.; Munoz, F.; and Joly, A. 2022. Deep Species Distribution Modeling From Sentinel-2 Image Time-Series: A Global Scale Analysis on the Orchid Family. *Frontiers in Plant Science*, 13: 839327.
- Fick, S. E.; and Hijmans, R. J. 2017. WorldClim 2: new 1-km spatial resolution climate surfaces for global land areas. *Int. Journal of Climatology*, 37(12): 4302–4315.
- Fink, D.; Auer, T.; Johnston, A.; Ruiz-Gutierrez, V.; Hochachka, W. M.; and Kelling, S. 2020. Modeling avian full annual cycle distribution and population trends with citizen science data. *Ecological Applications*, 30(3): e02056.
- Gal, Y.; and Ghahramani, Z. 2016. Dropout as a Bayesian Approximation: Representing Model Uncertainty in Deep Learning. In *Proc. of The 33rd International Conference on Machine Learning*, 1050–1059.
- Golding, N.; and Purse, B. V. 2016. Fast and flexible Bayesian species distribution modelling using Gaussian processes. *Methods in Ecology and Evolution*, 7(5): 598–608.
- Goodfellow, I.; Bengio, Y.; and Courville, A. 2016. *Deep Learning*. MIT Press.
- Guisan, A.; Edwards, T. C.; and Hastie, T. 2002. Generalized linear and generalized additive models in studies of species distributions: setting the scene. *Ecological Modelling*, 157(2): 89–100.
- Guo, C.; Lek, S.; Ye, S.; Li, W.; Liu, J.; and Li, Z. 2015. Uncertainty in ensemble modelling of large-scale species distribution: Effects from species characteristics and model techniques. *Ecological Modelling*, 306: 67–75.
- Hamilton, M.; Lange, C.; Cole, E.; Shepard, A.; Heinrich, S.; Mac Aodha, O.; Van Horn, G.; and Maji, S. 2024. Combining Observational Data and Language for Species Range Estimation. In *Advances in Neural Information Processing Systems*, 17719–17742.
- Hazen, E. L.; Scales, K. L.; Maxwell, S. M.; Briscoe, D. K.; Welch, H.; Bograd, S. J.; Bailey, H.; Benson, S. R.; Eguchi, T.; Dewar, H.; Kohin, S.; Costa, D. P.; Crowder, L. B.; and Lewison, R. L. 2018. A dynamic ocean management tool to reduce bycatch and support sustainable fisheries. *Science Advances*, 4(5): eaar3001.
- He, K.; Zhang, X.; Ren, S.; and Sun, J. 2016. Deep Residual Learning for Image Recognition. In *Proc. of the IEEE Conference on Computer Vision and Pattern Recognition (CVPR)*.
- iNaturalist. n.d. <https://www.inaturalist.org/>. Accessed: 2025-05-01.
- Jetz, W.; McGeoch, M. A.; Guralnick, R.; Ferrier, S.; Beck, J.; Costello, M. J.; Fernandez, M.; Geller, G. N.; Keil, P.; Merow, C.; Meyer, C.; Muller-Karger, F. E.; Pereira, H. M.; Regan, E. C.; Schmeller, D. S.; and Turak, E. 2019. Essential biodiversity variables for mapping and monitoring species populations. *Nature Ecology & Evolution*, 3(4): 539–551.
- Johnston, A.; Hochachka, W. M.; Strimas-Mackey, M. E.; Ruiz Gutierrez, V.; Robinson, O. J.; Miller, E. T.; Auer, T.; Kelling, S. T.; and Fink, D. 2021. Analytical guidelines to increase the value of community science data: An example using eBird data to estimate species distributions. *Diversity and Distributions*, 27(7): 1265–1277.
- Kadmon, R.; Farber, O.; and Danin, A. 2004. Effect of Roadside bias On The Accuracy Of Predictive Maps Produced By Bioclimatic Models. *Ecological Applications*, 14(2): 401–413.
- Kendall, A.; Badrinarayanan, V.; and Cipolla, R. 2016. Bayesian SegNet: Model Uncertainty in Deep Convolutional Encoder-Decoder Architectures for Scene Understanding. arXiv:1511.02680.
- Kendall, A.; and Gal, Y. 2017. What uncertainties do we need in Bayesian deep learning for computer vision? In *Proc. of the 31st International Conference on Neural Information Processing Systems*, 5580–5590.
- Kingma, D. P. 2014. Adam: A method for stochastic optimization. arXiv:1412.6980.
- Krizhevsky, A. 2009. *Learning Multiple Layers of Features from Tiny Images*. Master's thesis, Department of Computer Science, University of Toronto.
- Lakshminarayanan, B.; Pritzel, A.; and Blundell, C. 2017. Simple and scalable predictive uncertainty estimation using deep ensembles. In *Proc. of the 31st International Conference on Neural Information Processing Systems*, 6405–6416.
- Lange, C.; Cole, E.; Van Horn, G.; and Mac Aodha, O. 2023. Active Learning-Based Species Range Estimation. In *Advances in Neural Information Processing Systems*, 41892–41913.
- Lange, C.; Hamilton, M.; Cole, E.; Shepard, A.; Heinrich, S.; Zhu, A.; Maji, S.; Horn, G. V.; and Aodha, O. M. 2025. Few-shot Species Range Estimation.
- Lee, S.; Purushwalkam, S.; Cogswell, M.; Crandall, D.; and Batra, D. 2015. Why M Heads are Better than One: Training a Diverse Ensemble of Deep Networks. arXiv:1511.06314.
- MacKenzie, D. I. 2018. *Occupancy estimation and modeling: inferring patterns and dynamics of species occurrence*. London: Academic Press, second edition edition.
- Mucsányi, B.; Kirchhof, M.; and Oh, S. J. 2024. Benchmarking Uncertainty Disentanglement: Specialized Uncertainties for Specialized Tasks. In *Advances in Neural Information Processing Systems*, 50972–51038.
- Mukhoti, J.; Kirsch, A.; van Amersfoort, J.; Torr, P. H.; and Gal, Y. 2021. Deterministic Neural Networks with Inductive Biases Capture Epistemic and Aleatoric Uncertainty. arXiv:2102.11582.
- Nix, D.; and Weigend, A. 1994. Estimating the mean and variance of the target probability distribution. In *Proc. of 1994 IEEE International Conference on Neural Networks*, 55–60.
- Omre, H.; Fjeldstad, T. M.; and Forberg, O. B. 2024. *Bayesian spatial modelling with conjugate prior models*. Springer.
- Phillips, S. J.; Dudík, M.; and Schapire, R. E. 2004. A maximum entropy approach to species distribution modeling. In *Twenty-first international Conference on Machine Learning*, 83.
- Roberts, D. R.; Bahn, V.; Ciuti, S.; Boyce, M. S.; Elith, J.; Guillera-Arroita, G.; Hauenstein, S.; Lahoz-Monfort, J. J.;

- Schröder, B.; Thuiller, W.; Warton, D. I.; Wintle, B. A.; Hartig, F.; and Dormann, C. F. 2017. Cross-validation strategies for data with temporal, spatial, hierarchical, or phylogenetic structure. *Ecography*, 40(8): 913–929.
- Rocchini, D.; Marcantonio, M.; Arhonditsis, G.; Cacciato, A. L.; Hauffe, H. C.; and He, K. S. 2019. Cartogramming uncertainty in species distribution models: A Bayesian approach. *Ecological Complexity*, 38: 146–155.
- Rocchini, D.; Tordoni, E.; Marchetto, E.; Marcantonio, M.; Barbosa, A. M.; Bazzichetto, M.; Beierkuhnlein, C.; Castelnovo, E.; Gatti, R. C.; Chiarucci, A.; Chieffallo, L.; Da Re, D.; Di Musciano, M.; Foody, G. M.; Gabor, L.; Garzon-Lopez, C. X.; Guisan, A.; Hattab, T.; Hortal, J.; Kunin, W. E.; Jordán, F.; Lenoir, J.; Mirri, S.; Moudry, V.; Naimi, B.; Nowosad, J.; Sabatini, F. M.; Schweiger, A. H.; Šímová, P.; Tassarolo, G.; Zannini, P.; and Malavasi, M. 2023. A quixotic view of spatial bias in modelling the distribution of species and their diversity. *npj Biodiversity*, 2(1): 10.
- Sharma, S.; Winner, K.; Pollock, L. J.; Thorson, J. T.; Mäkinen, J.; Merow, C.; Pedersen, E. J.; Chefira, K. F.; Portmann, J. M.; Iannarilli, F.; Beery, S.; De Lutio, R.; and Jetz, W. 2025. No species left behind: borrowing strength to map data-deficient species. *Trends in Ecology & Evolution*, 40(7): 699–711.
- Sierra, E.; Gillespie, L. E.; Soltani, S.; Exposito-Alonso, M.; and Kattenborn, T. 2025. DivShift: Exploring Domain-Specific Distribution Shifts in Large-Scale, Volunteer-Collected Biodiversity Datasets. In *Proc. of the AAAI Conference on Artificial Intelligence*, 28386–28396.
- Sluijterman, L.; Cator, E.; and Heskes, T. 2023. Optimal Training of Mean Variance Estimation Neural Networks. arXiv:2302.08875.
- Speed, J. D. M.; Bendiksby, M.; Finstad, A. G.; Hassel, K.; Kolstad, A. L.; and Prestø, T. 2018. Contrasting spatial, temporal and environmental patterns in observation and specimen based species occurrence data. *PLOS One*, 13(4): e0196417.
- Sullivan, B. L.; Wood, C. L.; Iliff, M. J.; Bonney, R. E.; Fink, D.; and Kelling, S. 2009. eBird: A citizen-based bird observation network in the biological sciences. *Biological Conservation*, 142(10): 2282–2292.
- Syfert, M. M.; Joppa, L.; Smith, M. J.; Coomes, D. A.; Bachman, S. P.; and Brummitt, N. A. 2014. Using species distribution models to inform IUCN Red List assessments. *Biological Conservation*, 177: 174–184.
- Teng, M.; Elmustafa, A.; Akera, B.; Bengio, Y.; Radi, H.; Larochelle, H.; and Rolnick, D. 2023. SatBird: a Dataset for Bird Species Distribution Modeling using Remote Sensing and Citizen Science Data. In *Advances in Neural Information Processing Systems*, 75925–75950.
- Thuiller, W.; Pollock, L. J.; Gueguen, M.; and Münkemüller, T. 2015. From species distributions to meta-communities. *Ecology Letters*, 18(12): 1321–1328.
- Valavi, R.; Elith, J.; Lahoz-Monfort, J. J.; and Guillerá-Arroita, G. 2021. Modelling species presence-only data with random forests. *Ecography*, 44(12): 1731–1742.
- Van Proosdij, A. S. J.; Sosef, M. S. M.; Wieringa, J. J.; and Raes, N. 2016. Minimum required number of specimen records to develop accurate species distribution models. *Ecography*, 39(6): 542–552.
- Yates, K. L.; Bouchet, P. J.; Caley, M. J.; Mengersen, K.; Randin, C. F.; Parnell, S.; Fielding, A. H.; Bamford, A. J.; Ban, S.; Barbosa, A. M.; Dormann, C. F.; Elith, J.; Embling, C. B.; Ervin, G. N.; Fisher, R.; Gould, S.; Graf, R. F.; Gregr, E. J.; Halpin, P. N.; Heikkinen, R. K.; Heinänen, S.; Jones, A. R.; Krishnakumar, P. K.; Lauria, V.; Lozano-Montes, H.; Mannocci, L.; Mellin, C.; Mesgaran, M. B.; Moreno-Amat, E.; Mormede, S.; Novacek, E.; Oppel, S.; Ortuño Crespo, G.; Peterson, A. T.; Rapacciuolo, G.; Roberts, J. J.; Ross, R. E.; Scales, K. L.; Schoeman, D.; Snelgrove, P.; Sundblad, G.; Thuiller, W.; Torres, L. G.; Verbruggen, H.; Wang, L.; Wenger, S.; Whittingham, M. J.; Zharikov, Y.; Zurell, D.; and Sequeira, A. M. 2018. Outstanding Challenges in the Transferability of Ecological Models. *Trends in Ecology & Evolution*, 33(10): 790–802.
- Zbinden, R.; van Tiel, N.; Kellenberger, B.; Hughes, L.; and Tuia, D. 2024. On the selection and effectiveness of pseudo-absences for species distribution modeling with deep learning. *Ecological Informatics*, 81: 102623.
- Zulian, V.; Miller, D. A. W.; and Ferraz, G. 2021. Integrating citizen-science and planned-survey data improves species distribution estimates. *Diversity and Distributions*, 27(12): 2498–2509.
- Zurell, D.; Franklin, J.; König, C.; Bouchet, P. J.; Dormann, C. F.; Elith, J.; Fandos, G.; Feng, X.; Guillerá-Arroita, G.; Guisan, A.; Lahoz-Monfort, J. J.; Leitão, P. J.; Park, D. S.; Peterson, A. T.; Rapacciuolo, G.; Schmatz, D. R.; Schröder, B.; Serra-Diaz, J. M.; Thuiller, W.; Yates, K. L.; Zimmermann, N. E.; and Merow, C. 2020. A standard protocol for reporting species distribution models. *Ecography*, 43(9): 1261–1277.

A Dataset

Input Variables

Satellite Imagery. We used remote sensing imagery from the Sentinel-2 satellite. Sentinel-2 data is publicly available and can be easily extracted with Google EarthEngine, using their `COPERNICUS/S2_SR_HARMONIZED` dataset from their Data Catalog. We provide code to extract Sentinel-2 data from EarthEngine in our Github repository. A summary of the bands we extracted (RGBNIR) can be found in Table 3. Each band has a resolution of 10m/pixel. We strictly considered images with a cloud coverage of up to 10%.

Sentinel-2 Bands		
Band	Description	Resolution
B4	Red	10m/pixel
B3	Green	10m/pixel
B2	Blue	10m/pixel
B8	Near-Infrared (NIR)	10m/pixel

Table 3: Description of the four bands we extracted from Sentinel-2 rasters

Bioclimatic Variables. We used the 19 bioclimatic variables of the WorldClim model Fick and Hijmans (2017). For the USA-Summer and USA-Winter subsets, we followed Teng et al. (2023); Cole et al. (2020) and considered data from WorldClim 1.4, which has data aggregated from 1960-1990. For Kenya and South Africa, we considered data from WorldClim 2.1 instead, which has data aggregated from 1970-2000. Both WorldClim 1.4 and WorldClim 2.1 share the same variables and the same resolution (approximately 1km per pixel). Table 4 summarizes the variables we used.

MLP/RF Inputs. The pipeline we leveraged to build model inputs for our MLP and Random Forest baselines is summarized by Algorithm 1.

Algorithm 1: Input Generation Pipeline for MLP and Random Forest baselines

Input : List of hotspots $\mathcal{H} = \{h_1, h_2, \dots, h_n\}$
Output : Processed model inputs for each hotspot
for each h_k in \mathcal{H} **do**
 Step 1 : Retrieve (lat, lon) coordinates associated with h_k from the eBird DataBase
 Step 2 : From (lat, lon) , retrieve an input vector $\mathbf{x}_k \in \mathbb{R}^{19}$ from WorldClim rasters
end for

Resnet-18 Inputs. The pipeline we leveraged to build model inputs for our Resnet18-based models is summarized by Algorithm 2. Note that the conversion to latitude/longitude coordinates to UTM projection system is a standard practice, as it allows Euclidean distances to be computed in meters. It therefore becomes straightforward to crop a region of a pre-determined size from any raster.

Algorithm 2: Input Generation Pipeline for Resnet18-based models

Input : List of hotspots $\mathcal{H} = \{h_1, h_2, \dots, h_n\}$
Output : Processed model inputs for each hotspot
for each h_k in \mathcal{H} **do**
 Step 1 : Retrieve (lat, lon) coordinates associated with h_k from the eBird DataBase
 Step 2 : Convert (lat, lon) coordinates into UTM projection (utm_e, utm_n)
 Step 3 : Build a 5km^2 bounding box centered on (utm_e, utm_n)
 Step 4 : Use the bounding box obtained from previous step to extract `sat_img` raster from Sentinel-2 and `env_var` raster from WorldClim
 Step 5 : Use bilinear interpolation to match `env_var` (1km/pixel) resolution to `sat_img` resolution (10m/pixel)
 Step 6 : From each (sat_img, env_var) pair, retrieve an input matrix $\mathbf{X}_k \in \mathbb{R}^{64 \times 64 \times 19}$ by center-cropping a region of 640m^2
end for

Splits

Table 5 describes the number of hotspots and the number of checklists associated with the four subsets of our dataset, for each split (train/val/test). These splits were obtained following the process described in section 4. Similarly to (Teng et al. 2023) and following recommendations in the literature (Roberts et al. 2017), we pre-processed the data based on the geospatial coordinates of each hotspot in order to prevent auto-correlation and over-fitting using DBSCAN to cluster hotspots within 5km of each other and ensuring that individual members of each cluster were proportionally distributed across splits.

Species List

Our dataset only considers the regularly occurring species for each region and exclude observations of very rare species (e.g. Eurasian birds occasionally blown by storms to the US), as such sightings are both unpredictable and do not generally provide any meaningful information about the ecosystem.

Kenya. We limited the species list to the 1054 species regularly found in Kenya according to Avibase (Avibase - The World Bird Database).

South Africa. We limited the species list to the 755 species regularly found in South Africa according to Bird Life South Africa (BirdLife - Bird Checklists of South Africa).

USA-Winter and USA-Summer. We limited the species list to the 670 species regularly found in continental United States according to the 2022 Checklist of the Continental United States from the American Birding Association (American Birding Association ; Checklists of the continental United States). More specifically, we only considered

Bioclimatic Variables		
Name	Description	Unit
bio_1	Annual Mean Temperature	°C
bio_2	Mean Diurnal Range (Mean of monthly (max temp - min temp))	°C
bio_3	Isothermality (BIO2/BIO7) (×100)	%
bio_4	Temperature Seasonality (standard deviation ×100)	°C
bio_5	Max Temperature of Warmest Month	°C
bio_6	Min Temperature of Coldest Month	°C
bio_7	Temperature Annual Range (BIO5-BIO6)	°C
bio_8	Mean Temperature of Wettest Quarter	°C
bio_9	Mean Temperature of Driest Quarter	°C
bio_10	Mean Temperature of Warmest Quarter	°C
bio_11	Mean Temperature of Coldest Quarter	°C
bio_12	Annual Precipitation	mm
bio_13	Precipitation of Wettest Month	mm
bio_14	Precipitation of Driest Month	mm
bio_15	Precipitation Seasonality	Coefficient of variation
bio_16	Precipitation of Wettest Quarter	mm
bio_17	Precipitation of Driest Quarter	mm
bio_18	Precipitation of Warmest Quarter	mm
bio_19	Precipitation of Coldest Quarter	mm

Table 4: Description of the bioclimatic variables extracted from WorldClim. Each of these rasters has a resolution of approximately 1km per pixel

	Training	Validation	Testing
Kenya			
N. Hotspots	6,481	1,852	218
N. Checklists	24,532	6,380	13,940
South Africa			
N. Hotspots	5,372	672	599
N. Checklists	137,740	12,051	349,076
USA-Winter			
N. Hotspots	26,422	5,747	17,173
N. Checklists	1,626,861	420,020	1,941,704
USA-Summer			
N. Hotspots	63,796	14,761	24,932
N. Checklists	1,721,678	477,490	1,895,054

Table 5: Composition of each split for each dataset

species denoted by ABA Codes 1 or 2, which include regular breeding species and visitors that are widespread across the country. We did not consider the species that are known to only occur in Alaska, Hawaii or the U.S. Territories (e.g. Guam, Puerto Rico, American Samoa, etc.).

Dataset Overview : Kenya

We provide a visual overview of the Kenya subdataset below. Figure 4 shows the geographical distribution of hotspots and species, as well as the distribution of non-zero encounter rates per hotspot.

Dataset Overview : USA-Winter

We provide a visual overview of the USA-Winter subdataset below. Figure 5 shows the geographical distribution

of hotspots and species, as well as the distribution of non-zero encounter rates per hotspot.

Dataset Overview : South Africa

We provide a visual overview of the South-Africa subdataset below. Figure 6 shows the geographical distribution of hotspots and species, as well as the distribution of non-zero encounter rates per hotspot.

Dataset Overview : USA-Summer

We provide a visual overview of the USA-Winter subdataset below. Figure 7 shows the geographical distribution of hotspots and species, as well as the distribution of non-zero encounter rates per hotspot.

B HuggingFace Repository

Our Dataset is available on HuggingFace. More information can be found in the README.md of the repository.

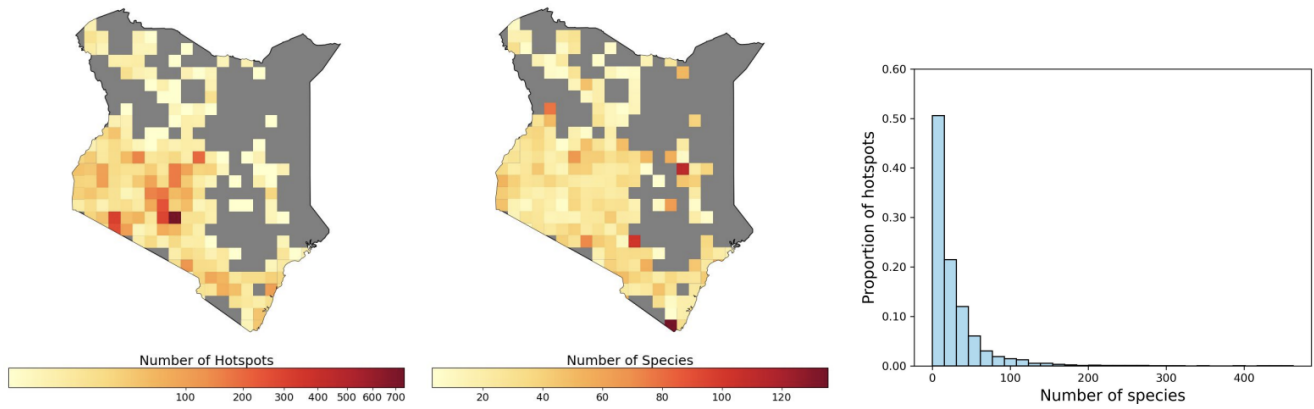
C Code Repository

Our Code is available on GitHub. More information can be found in the README.md of the repository.

D Licenses

The BATIS Benchmark is released under a Creative Commons Attribution-NonCommercial 4.0 International (CC BY-NC 4.0) License. The use of our dataset should comply with the eBird terms of Use, the eBird API Terms of use, and the eBird Data Access Terms of Use.

a



b

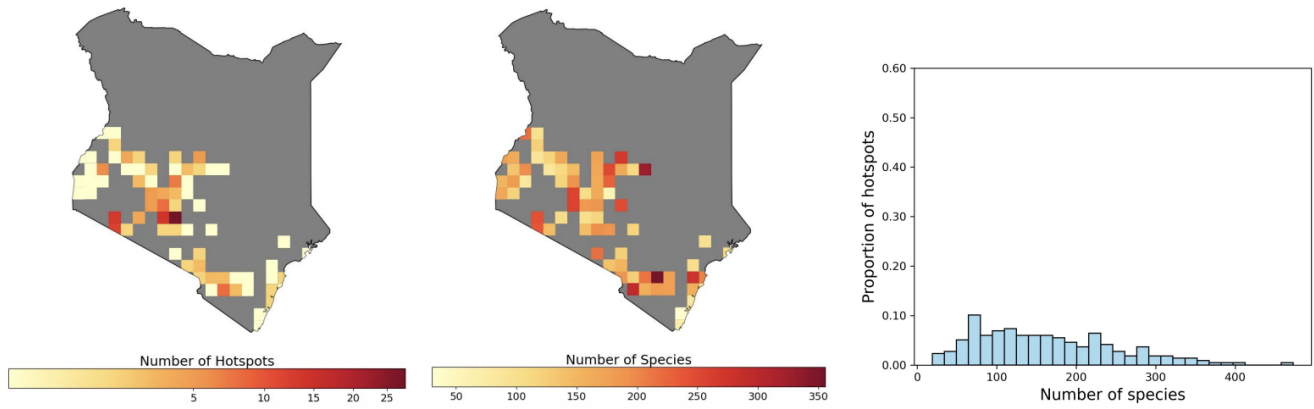


Figure 4: From left to right, for a) Training and b) Test : Geographical distribution of the total number of hotspots (left) and non-zero encounter rates (middle) associated with our Kenya subdataset, and distribution of the number of species encountered per hotspot (right).

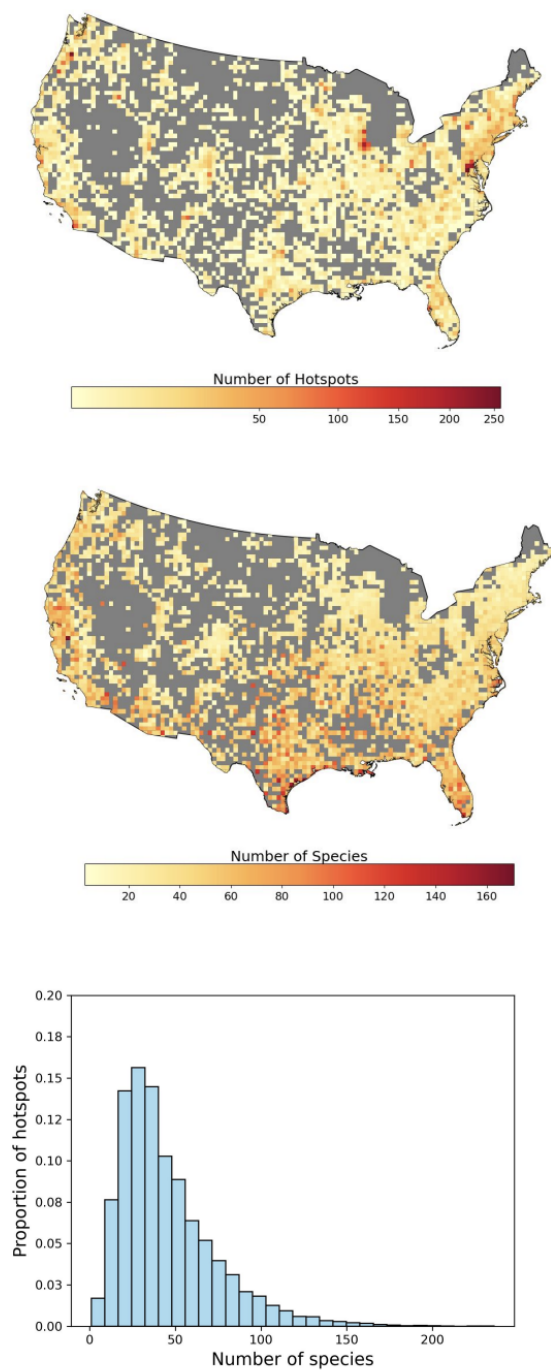
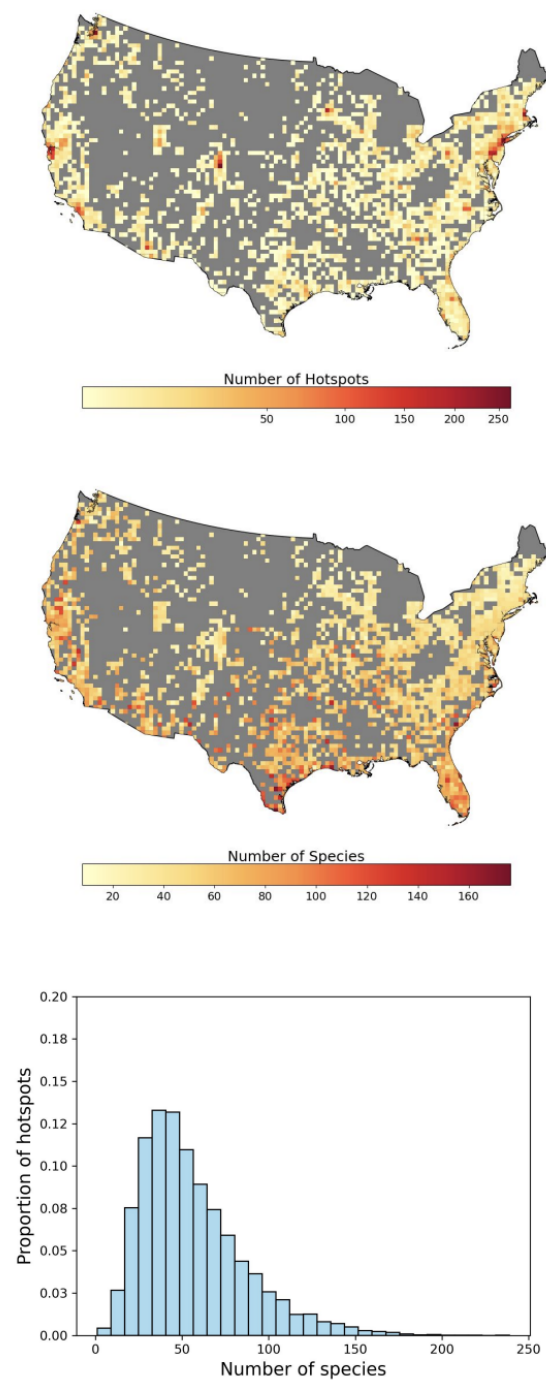
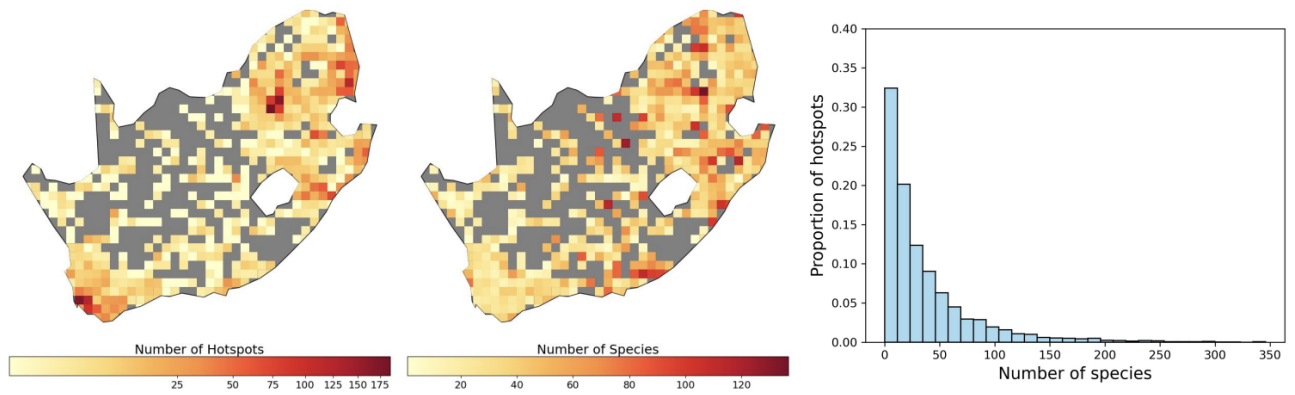
a**b**

Figure 5: From top to bottom, for a) Training and b) Test : Geographical distribution of the total number of hotspots (top) and non-zero encounter rates (middle) associated with our US-Winter subdataset, and distribution of the number of species encountered per hotspot (bottom).

a



b

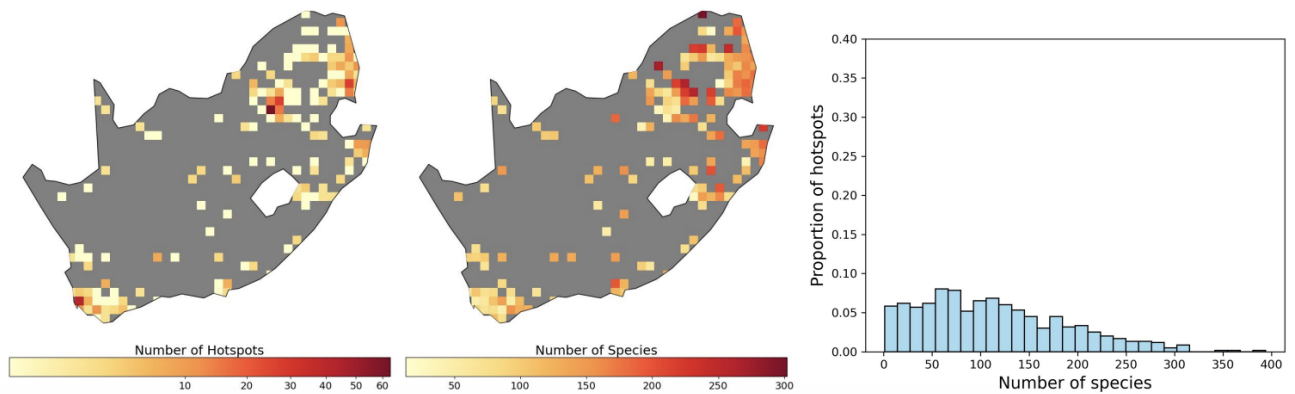


Figure 6: From left to right, for a) Training and b) Test : Geographical distribution of the total number of hotspots (left) and non-zero encounter rates (middle) associated with our South-Africa subdataset, and distribution of the number of species encountered per hotspot (right).

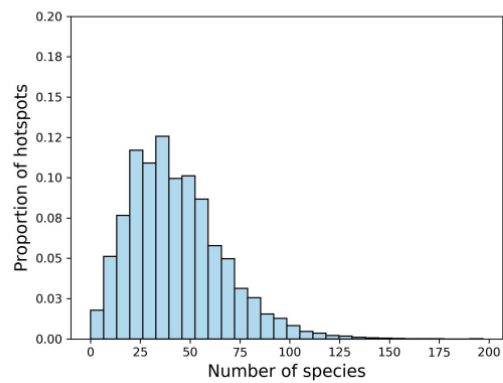
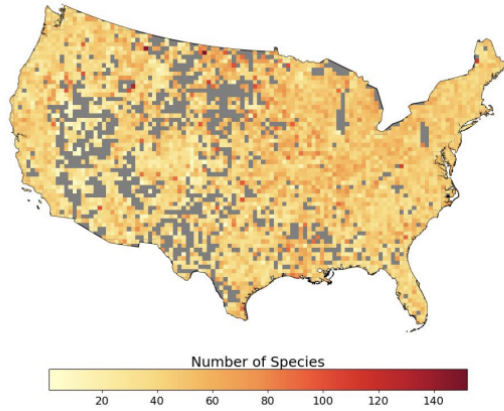
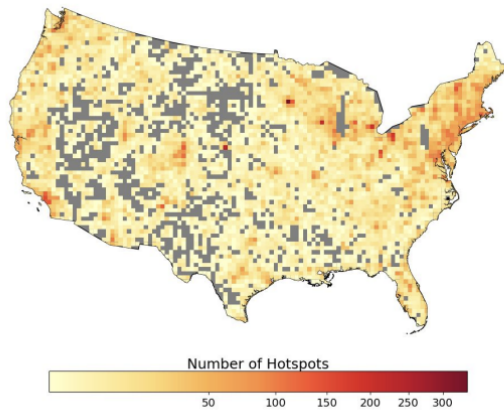
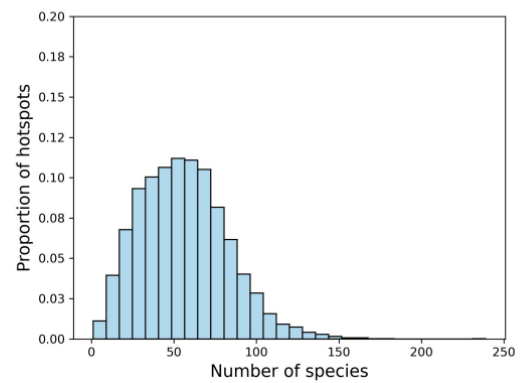
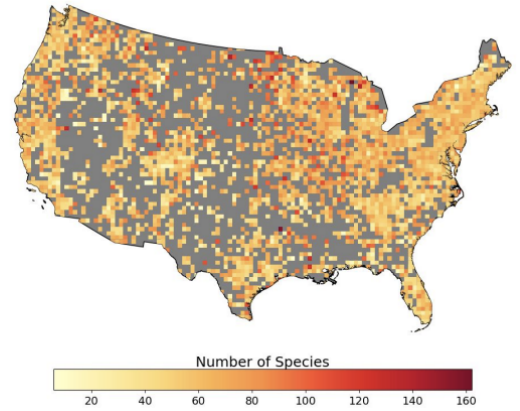
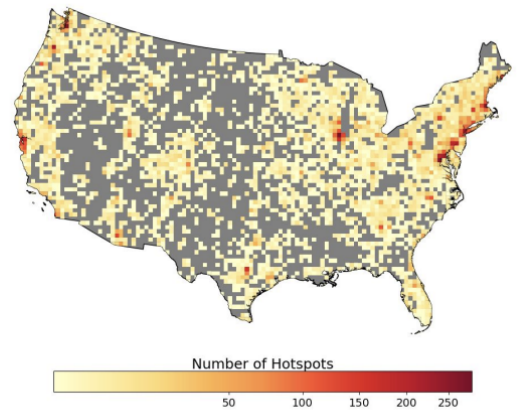
a**b**

Figure 7: From top to bottom, for a) Training and b) Test : Geographical distribution of the total number of hotspots (top) and non-zero encounter rates (middle) associated with our US-Sumer subdataset, and distribution of the number of species encountered per hotspot (bottom).

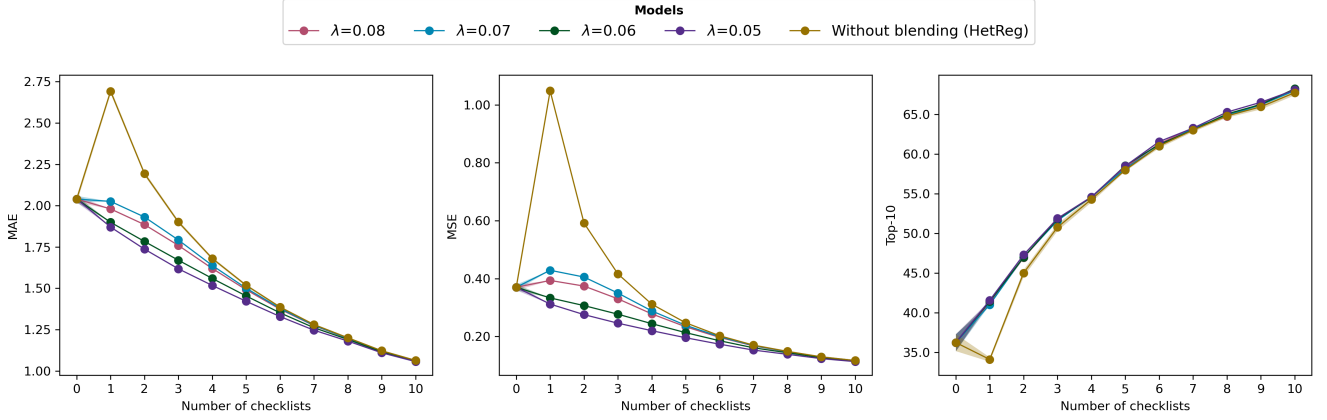


Figure 8: Iterative improvements of MAE, MSE and Top-10 metrics on the Kenya sub-dataset with increasing number of BATIS updates for our best performing uncertainty-aware model (HetReg), with and without progressive blending of prior and posterior predictions. Results are shown for various values for hyperparameter λ (see equation 6).

E Limitations

As shown in Figure 2, the initial predictions of an uncertainty-aware SDM can be overwritten in a first Bayesian update, when the estimated prior variance is large. This can lead to an initial drop in performance before enough updates are performed to boost performance, even though performance would ideally increase *monotonically* with number of updates. A simple approach to mitigate such behavior is to consider a weighted average of predictions from the prior and the updated SDM, progressively giving more importance to the updates with more observations. For example, we can consider blended predictions

$$p_{blend} = (1 - w_t) \cdot p_{prior} + w_t \cdot p_{posterior} \quad (6)$$

where $w_t \in (0, 1]$ is an appropriate discounting factor. A practical choice for w_t is $w_t = 1 - \exp^{-\lambda t}$, where t corresponds to the number of BATIS posterior updates and $\lambda \in (0, 1]$ is a tunable hyperparameter. Figure 8 illustrates how this strategy can progressively smooth performance curves for our best performing uncertainty-aware model (HetReg) on the Kenya sub-dataset.

F Methods

Uncertainty-agnostic methods

We give additional details below on the implementation of our uncertainty-agnostic methods. A summary of the hyperparameter values we used for each of these approaches can be found in Table 6.

Mean Encounter Rate. As described in the main paper, we simply computed the average of encounter rates over the training set for each species.

Random Forest. A Random Forest Regressor is an ensemble learning method that builds multiple decision trees during training and averages their predictions to improve accuracy and reduce overfitting. Each tree is trained on a random subset of the data, in order to diversity among

the models. Our Random Forest baseline uses 100 trees, and clips the output between $[0, 1]$ to predict the encounter rate. To implement this baseline, we simply used the `RandomForestRegressor` class from the `scikit-learn` library.

Multi-Layer Perceptron. A Multi-Layer Perceptron (MLP) is a simple feedforward neural network consisting of an input layer, one or more hidden layers, and an output layer (Goodfellow, Bengio, and Courville 2016). We used a single hidden layer of dimension 64 and sigmoid activation layers. The MLP was trained with the binary cross-entropy loss, i.e.

$$\mathcal{L}_{CE} := \frac{1}{N} \sum_{i=1}^N -\mathbf{y}_i \log(\hat{\mathbf{y}}_i) - (1 - \mathbf{y}_i) \log(1 - \hat{\mathbf{y}}_i) \quad (7)$$

where N corresponds to the number of hotspots in a given batch, \mathbf{y}_i corresponds the ground encounter rate vector of hotspot $h_i \in \mathcal{H}$, and $\hat{\mathbf{y}}_i$ corresponds to the predicted encounter rate vector.

Resnet-18. We used a conventional Resnet-18 architecture (He et al. 2016), initialized with weights pre-trained on ImageNet. The model was trained with the binary cross-entropy loss (equation 7), and implemented in Pytorch with the help of the `torchvision.models.resnet18` class.

Parameter	Description	Assigned value
Random Forest		
n_tree	Number of trees	100
Multi-Layer Perceptron		
n_layers	Number of hidden layers	1
layer_size	Size of hidden layer(s)	64

Table 6: Summary of hyperparameter values used to train our uncertainty-agnostic methods

Uncertainty-aware methods

We give additional details below on the implementation of our Monte-Carlo Dropout, Mean-Variance Network and Heteroscedastic Regression Neural Network. Sufficient details are provided in the main paper for the other approaches. A summary of the hyperparameter values we used for each of our uncertainty-aware methods can be found in Table 7.

Monte-Carlo Dropout. Monte-Carlo Dropout (MCD) randomly deactivates a proportion ρ of neurons at training and test time, and uses M forward passes to compute the mean and variance for each hotspot. Dropout layers need to be carefully placed, as they can quickly degrade accuracy for large models, which will dramatically increase the computation time required to achieve a satisfying performance (Kendall, Badrinarayanan, and Cipolla 2016). We did the same as (Kendall and Gal 2017) and added only a single dropout layer before the last layer of the network.

Mean-Variance Network. A Mean-Variance Network (MVN) maps each location to two outputs: a predicted mean encounter rate vector and a predicted variance vector. It does so by using the **Gaussian negative log-likelihood function**, i.e.

$$\mathcal{L}_{GL} := \frac{1}{N} \sum_{i=1}^N \frac{1}{2} \log \hat{\sigma}_i^2 + \frac{(\mathbf{y}_i - \hat{\mathbf{y}}_i)^2}{2\hat{\sigma}_i^2} \quad (8)$$

where N corresponds to the number of hotspots in a given batch, \mathbf{y}_i corresponds to the ground truth encounter rate vector of hotspot $h_i \in \mathcal{H}$, and $\hat{\mathbf{y}}_i^2$ and $\hat{\sigma}_i^2$ respectively corresponds to the predicted encounter rate and variance vectors.

In order to optimize performance, we followed recommendations formulated in (Sluijterman, Cator, and Heskes 2023) and added a separate regularization of the mean and the variance estimate. Our loss function therefore became

$$\begin{aligned} \mathcal{L}_{GLT} := & \frac{1}{N} \sum_{i=1}^N \left[\frac{1}{2} \log \hat{\sigma}_i^2 + \frac{(\mathbf{y}_i - \hat{\mathbf{y}}_i)^2}{2\hat{\sigma}_i^2} \right] \\ & + \lambda_\mu \frac{1}{N} \sum \hat{\mathbf{y}}_i^2 + \lambda_\sigma \frac{1}{N} \sum \log(\hat{\sigma}_i^2) \end{aligned} \quad (9)$$

where λ_μ and λ_σ are tunable hyperparameters. The λ_μ parameter penalizes very large predictions, and λ_σ prevent the model from being over or under-confident.

Another choice we made to optimize training is to add a **warm-up period** at the beginning, to prevent the model from minimizing the loss by maximizing the variance at the start. We do so by simply setting $\hat{\sigma}_i^2 = 1$ for a pre-determined number of epochs at the start.

Heteroscedastic Regression Neural Network (Kendall and Gal 2017). A Heteroscedastic Regression Neural Network (HetReg) is very similar to an MVN, but adds MC Dropout sampling to simultaneously quantify aleatoric and epistemic uncertainty. M dropout passes are used to compute the mean encounter rate vector, and variance is estimated by adding epistemic uncertainty (variance computed from M predicted encounter rates) to aleatoric uncertainty (mean computed from M predicted variances).

We applied the same optimizations to HetReg than to MVN, and we implemented dropout the same way as we did for our MCD baseline.

G Experiments

Training protocol.

All deep learning models were trained using the Adam (Kingma 2014) optimizer, with a batch size of 128 and for a maximum of 50 epochs. We trained each model with three different seeds, and we used 30 dropout pass at test time to compute the mean and variance of predictions for the approaches requiring a dropout layer to quantify uncertainty (Gal and Ghahramani 2016). Random noise, blur and vertical/horizontal flipping were used for data augmentation, and we normalized inputs (satellite imagery and/or bioclimatic variables) using training set statistics. The optimizer hyperparameter values we used in each of our experiments are listed in Table 8. In addition, a summary of the hyperparameter values we used for each of our uncertainty-aware methods can be found in Table 7.

We report results generated with the same learning rate (0.0001) for all Resnet18-based models because it was demonstrated to be the one that gave the best results in the related SatBird task (Teng et al. 2023). For our Monte-Carlo Dropout approach, we took inspiration from the experiments in Gal and Ghahramani (2016) and considered $\rho = 0.2$ as the dropout rate for MCD and HetReg. For the warmup, λ_μ and λ_σ hyperparameters of our Mean-Variance Network and HetReg approaches, we considered warmup = [2, 5, 10], $\lambda_\mu = [0.1, 0.001, 0.0001]$, $\lambda_\sigma = [0.1, 0.001, 0.0001]$, and found that using warmup = 5, $\lambda_\mu = 0.1$ and $\lambda_\sigma = 0.1$ led to the best results.

Random Seeds. For each individual experiment, we used a random number generator to generate on seed number, which was then used to set `numpy.random.seed`, `random.seed` and `torch.manual.seed`. The generated seed can then be re-used for reproducibility of a single experiment if needed. For each model in our benchmark, we showed results averaged from 3 different random seeds (i.e., we trained each model 3 different times).

Metrics

Let N be the number of species, \mathcal{H} be a set of hotspots, y_i be the ground truth encounter rate vector for species i at hotspot $h \in \mathcal{H}$, \hat{y}_i be the predicted encounter rate for species i at hotspot $h \in \mathcal{H}$. Our metrics are defined as follows :

Mean Absolute Error (MAE). The MAE for a single hotspot $h \in \mathcal{H}$ is defined as

$$\text{MAE} := \frac{1}{N} \sum_{i=1}^N |y_i - \hat{y}_i| \quad (10)$$

Mean Squared Error (MSE). The MSE for a single hotspot $h \in \mathcal{H}$ is defined as

$$\text{MSE} := \frac{1}{N} \sum_{i=1}^N (y_i - \hat{y}_i)^2 \quad (11)$$

Adaptive Top-k. Our Top- k metric measures how well the model’s top- k predicted species (those it expects to be the most frequently encountered) align with the ground truth

Hyperparameter	Description	Assigned value
Resnet-18 + Fixed Variance		
τ	Scaling Parameter for the Variance	1
Resnet-18+Historical Variance		
edge_case	Value to assign to variance when historical variance is too high	$\mu \cdot (1 - \mu)$
Resnet-18 + Mean-Variance Network		
λ_μ	Regularization parameter for predicted mean	0.1
λ_σ	Regularization parameter for predicted variance	0.1
warmup	Number of epochs to warmup model	5
Resnet-18 + Dropout		
ρ	Dropout rate	0.2
M	Number of dropout passes to compute predicted mean and variance	30
Resnet-18 + HetReg		
λ_μ	Regularization parameter for mean	0.1
λ_σ	Regularization parameter for variance	0.1
warmup	Number of epochs to warmup model	5
ρ	Dropout rate	0.2
M	Number of dropout passes to compute predicted mean and variance	30
Resnet-18 + Deep Ensembles		
M	Number of independently trained models from which to compute predicted mean and variance	5
Resnet-18 + Shallow Ensembles		
M	Number of heads	5

Table 7: Summary of hyperparameter values used to train our uncertainty-aware methods

Hyperparameter	Description	Assigned value
Multi-Layer Perceptron		
learning_rate	Learning Rate (for Adam)	0.001
batch_size	Batch size	128
max_epochs	Maximum number of epochs to train the model	50
factor	Reduction factor for the learning rate if validation loss does not improve for patience epochs	0.5
patience	Number of successive epochs to monitor change in validation loss	20
Resnet18-based Models		
learning_rate	Number of hidden layers (for Adam)	0.0001
weight_decay	L2 Regularization (for Adam)	0.00001
batch_size	Maximum number of epochs to train the model	128
max_epochs	Maximum number of epochs to train the model	50
factor	Reduction factor for the learning rate if validation loss does not improve for patience epochs	0.5
patience	Number of successive epochs to monitor change in validation loss	20

Table 8: Summary of hyperparameter values used to parametrize our model training protocol

top- k species encountered in the field. This metric can be formally defined as

$$\text{Top-}k := \begin{cases} \frac{|\mathcal{I}_{\hat{y}} \cap \mathcal{I}_y|}{k} \cdot 100 & \text{if } k > 0 \\ 0 & \text{otherwise} \end{cases} \quad (12)$$

where $k = |i : y_i \neq 0|$ denotes the number of non-zero ground truth encounter rates at hotspot $h \in \mathcal{H}$, $\mathcal{I}_{\hat{y}}$ denotes the sets of indices of the top- k largest values in $\hat{\mathbf{y}}$, and \mathcal{I}_y denotes the sets of indices of the top- k largest values in \mathbf{y} .

A top- k score of 100% means the model perfectly identified all of the k most commonly encountered species at

hotspot $h \in \mathcal{H}$, and a score of 0 indicates that none of the top- k predicted species matched the ground truth top- k species.

Top-10 and Top-30. Adaptive Top-10 and Top-30 are defined similarly as top- k , except that k is respectively replaced by 10 or 30.

Python Environment

Our code was developed in Python 3.10. The required packages can be installed using the `requirements.txt` file provided in our Github repository.

Resources	Subset			
	Kenya	South-Africa	USA-Winter	USA-Summer
Resnet-18, Resnet+HetReg, Resnet+MVN, Resnet+MCD, Resnet+SE, Resnet+DE				
time	10:00:00	12:00:00	23:59:00	23:59:00
node	1	1	1	1
mem	24G	24G	24G	24G
cpus-per-task	1	1	1	1
gpus-per-node	1	1	1	1

Table 9: Summary of computing resources required by our job scripts for the four subsets of our dataset. Our Mean Encounter Rate, Random Forest and Multi-Layer Perceptron baselines were not trained on SLURM-based clusters.

Execution Environment

We validated that all our code can be executed on :

- SLURM-based clusters
- macOS Sonoma 14.1 (with Apple M Series chips)
- Windows 11 (with NVIDIA GeForce RTX 4070)

Model Training (Resnet-18). Resnet-18 models were trained independently on a computer cluster equipped with NVIDIA V100 GPUs (16 GB). The cluster we used rely on the open-source SLURM job scheduler, which is used by many of the world’s supercomputers. Our code environment should therefore work in other similar computer clusters. A summary of the computing resources our job scripts are requiring can be found in Table 9.

Model Training (Baselines). We trained our Mean Encounter Rate, Random Forest and Multi-Layer Perceptron baselines on a MacBook Pro equipped with an Apple M3 Pro Chip (18 GB), running on macOS Sonoma 14.1.

Bayesian Updating Framework. We performed the Bayesian Updating Framework experiments on a MacBook Pro equipped with an Apple M3 Pro Chip (18 GB), running on macOS Sonoma 14.1.

H Results

Additional Results for Kenya

Iterative Improvements by Region . Figure 9 shows the evolution of the performance of uncertainty-aware approaches with increasing number of checklist updates, on the Kenya subdataset. We can observe the same trends as Figure 2 of the main paper.

Results for USA-Summer

Overall. Table 10 shows results for the USA-Winter subdataset.

Iterative Improvements by Region . Figure 10 shows the evolution of the performance of uncertainty-aware approaches with increasing number of checklist updates, on the USA-Summer subdataset. We can observe the same trends as Figure 2 of the main paper.

Results for USA-Winter

Overall. Table 11 shows results for the USA-Winter subdataset.

Iterative Improvements by Region . Figure 11 shows the evolution of the performance of uncertainty-aware approaches with increasing number of checklist updates, on the Kenya subdataset. We can observe the same trends as Figure 2 of the main paper.

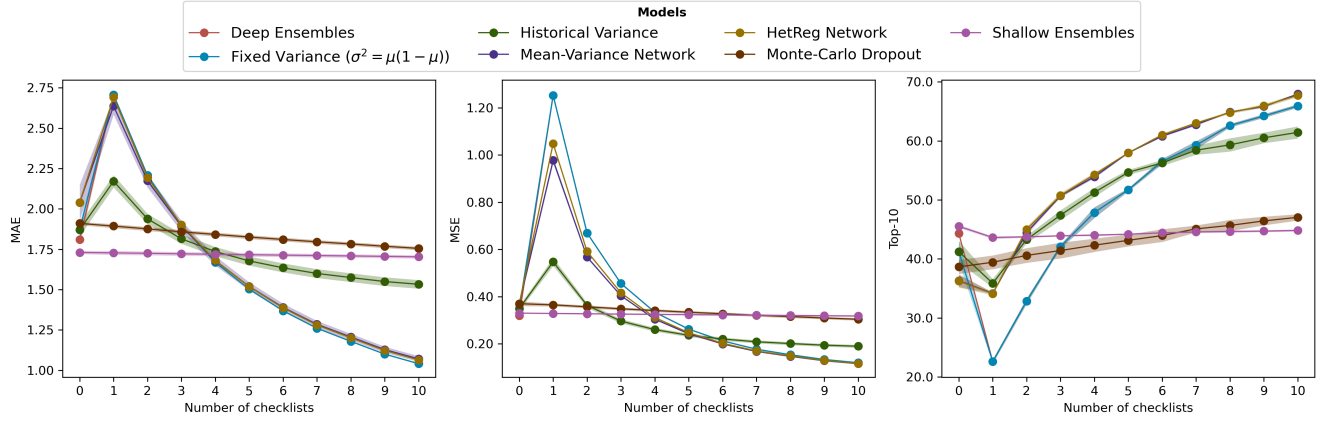


Figure 9: Iterative improvements for the different uncertainty estimation approaches with increasing number of checklist updates for the MAE, MSE and Top-10 metrics on the Kenya Region test set. We report the mean on three seeds and standard deviations for each model.

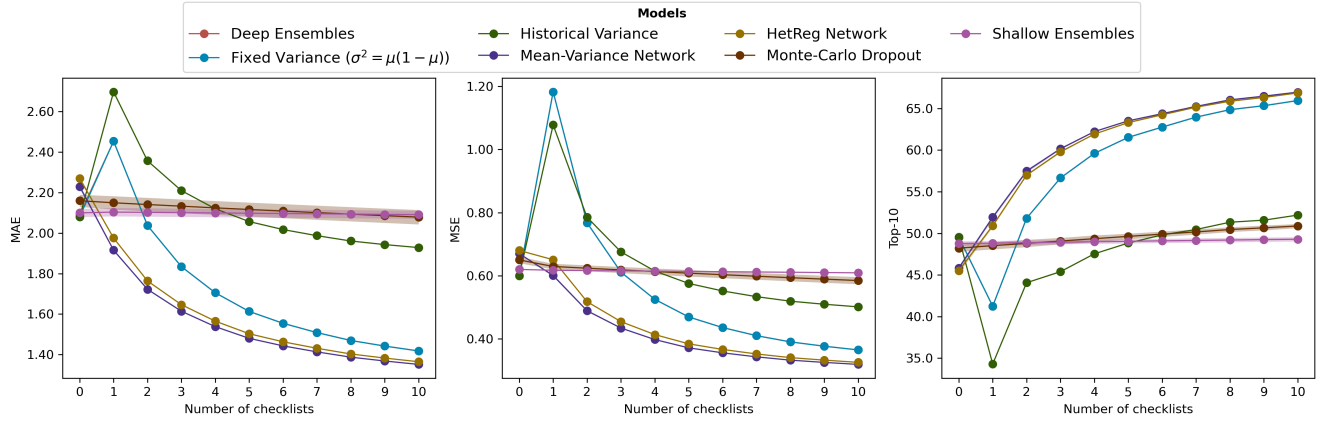


Figure 10: Iterative improvements for the different uncertainty estimation approaches with increasing number of checklist updates for the MAE, MSE and Top-10 metrics on the USA-Summer Region test set. We report the mean on three seeds and standard deviations for each model.

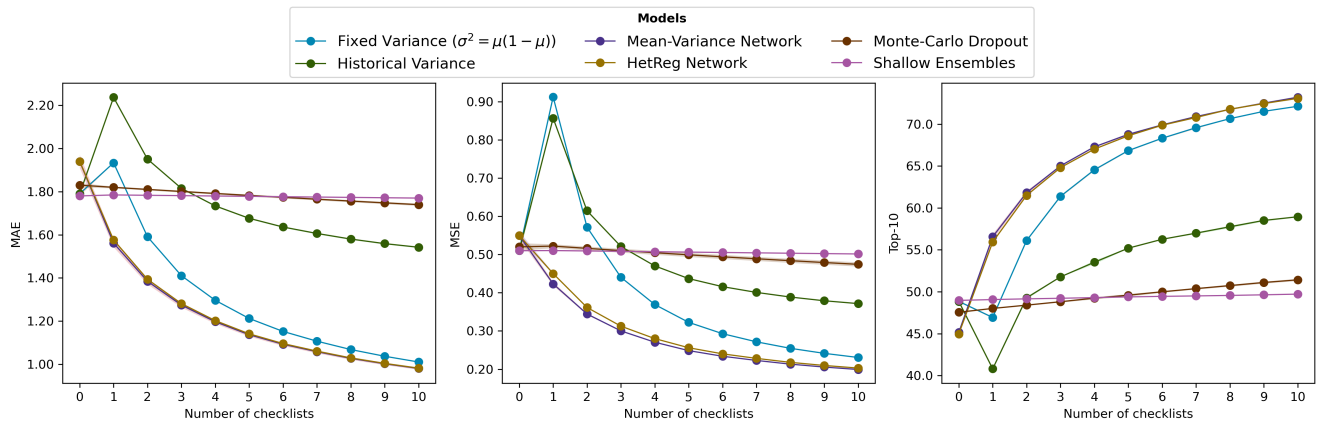


Figure 11: Iterative improvements for the different uncertainty estimation approaches with increasing number of checklist updates for the MAE, MSE and Top-10 metrics on the USA-Winter Region test set. We report the mean on three seeds and standard deviations for each model.

Model	Metrics									
	MAE[1e-2]		MSE[1e-2]		Top-10		Top-30		Top-k	
USA-Summer										
Mean Encounter Rate	3.08		0.91		29.69		45.47		51.97	
	±0.00		±0.00		±0.00		±0.00		±0.00	
MLP	2.29		0.66		44.18		62.27		69.04	
	±0.01		±0.00		±0.12		±0.03		±0.01	
Random Forest	1.96		0.59		49.38		67.07		72.44	
	±0.00		±0.00		±0.04		±0.02		±0.01	
ResNet-18	2.08		0.60		49.52		66.28		78.45	
	±0.00		±0.00		±0.05		±0.01		±0.01	
ResNet-18+FV	2.08	1.61	0.60	0.47	49.52	61.53	66.28	75.69	78.45	80.49
	±0.00	±0.00	±0.00	±0.00	±0.05	±0.01	±0.01	±0.01	±0.01	±2=00.00
ResNet-18+HV	2.08	2.06	0.60	0.57	49.52	48.83	66.28	69.79	78.45	75.56
	±0.00	±0.00	±0.00	±0.00	±0.04	±0.04	±0.01	±0.02	±0.01	±0.02
ResNet-18+DE	2.09	2.05	0.60	0.57	49.54	50.81	66.34	67.37	78.47	78.81
	±0.00	±0.06	±0.01	±0.00	±0.02	±0.01	±0.01	±0.01	±0.01	±0.00
ResNet-18+SE	2.10	2.09	0.62	0.61	48.78	49.04	65.62	65.81	78.04	78.08
	±0.02	±0.02	±0.00	±0.00	±0.27	±0.25	±0.21	±0.19	±0.15	±0.14
ResNet-18+MCD	2.16	2.11	0.65	0.60	48.22	49.63	64.83	66.05	77.43	77.81
	±0.03	±0.03	±0.01	±0.01	±0.43	±0.33	±0.00	±0.61	±0.26	±0.35
ResNet-18+MVN	2.23	1.48	0.67	0.37	45.83	63.51	62.77	76.02	76.18	78.14
	±0.01	±0.00	±0.00	±0.00	±0.24	±0.02	±0.04	±0.04	±0.02	±0.11
ResNet-18+HetReg	2.27	1.50	0.68	0.38	45.49	63.22	62.23	75.79	75.75	77.23
	±0.01	±0.00	±0.00	±0.00	±0.29	±0.12	±0.21	±0.02	±0.08	±0.10

Table 10: Performance of SDM-estimation approaches both **without Bayesian updates** (left side in split columns) and **after updates from five checklists** (right side). Note that the first four methods for each region are not uncertainty-aware and therefore cannot be updated with checklist information. Means are shown \pm standard deviation across runs. (Note that many standard deviations are quite low; those reported as 0.00 are accurate.)

Model	Metrics									
	MAE[1e-2]		MSE[1e-2]		Top-10		Top-30		Top-k	
USA-Winter										
Mean Encounter Rate	2.47		0.71		28.75		50.06		55.20	
	±0.00		±0.00		±0.00		±0.00		±0.00	
MLP	1.96		0.55		45.25		64.83		72.27	
	±0.01		±0.00		±0.14		±0.13		±0.06	
Random Forest	1.75		0.52		49.61		67.82		74.46	
	±0.00		±0.00		±0.06		±0.02		±0.04	
ResNet-18	1.79		0.51		48.85		67.62		75.13	
	±0.01		±0.00		±0.08		±0.09		±0.16	
ResNet-18+FV	1.79	1.21	0.51	0.32	48.85	66.83	67.62	77.56	75.13	78.13
	±0.01	±0.00	±0.00	±0.00	±0.08	±0.08	±0.09	±0.05	±0.16	±0.13
ResNet-18+HV	1.79	1.67	0.51	0.44	48.85	55.20	67.62	71.31	75.13	72.37
	±0.01	±0.01	±0.00	±0.00	±0.08	±0.03	±0.09	±0.05	±0.16	±0.10
ResNet-18+DE	1.77	1.75	0.50	0.48	49.55	51.77	68.11	69.40	75.80	70.41
	±0.01	±0.06	±0.00	±0.01	±0.01	±1.06	±0.03	±1.48	±0.01	±0.56
ResNet-18+SE	1.78	1.78	0.51	0.51	48.97	49.39	67.68	67.88	75.21	75.25
	±0.00	±0.00	±0.00	±0.00	±0.03	±0.02	±0.11	±0.11	±0.16	±0.17
ResNet-18+MCD	1.83	1.78	0.52	0.49	47.56	49.59	66.73	67.85	74.69	75.04
	±0.00	±0.00	±0.00	±0.00	±0.10	±0.15	±0.01	±0.03	±0.04	±0.03
ResNet-18+MVN	1.94	1.14	0.55	0.25	45.16	68.77	64.89	77.94	72.61	76.50
	±0.03	±0.01	±0.01	±0.00	±0.22	±0.11	±0.29	±0.11	±0.29	±0.28
ResNet-18+HetReg	1.94	1.14	0.55	0.26	44.97	68.60	64.88	77.86	72.49	76.33
	±0.00	±0.00	±0.00	±0.00	±0.02	±0.04	±0.11	±0.01	±0.03	±0.02

Table 11: Performance of SDM-estimation approaches both **without Bayesian updates** (left side in split columns) and **after updates from five checklists** (right side). Note that the first four methods for each region are not uncertainty-aware and therefore cannot be updated with checklist information. Means are shown \pm standard deviation across runs. (Note that many standard deviations are quite low; those reported as 0.00 are accurate.)